Mapping phytoplankton iron utilization: Insights into Southern Ocean supply mechanisms

P. W. Boyd,[1,2] K. R. Arrigo,[3] R. Strzepek,[4] and G. L. van Dijken[3]

Received 30 October 2011; revised 5 April 2012; accepted 25 April 2012; published 12 June 2012.

[1] The emerging field of ocean iron biogeochemistry has prompted interest in the identification and quantification of Fe supply mechanisms. However, less attention has been given to estimating biological Fe utilization, and using the magnitude of Fe utilization to enhance our understanding of modes of supply. Here, we combine regionally validated data sets (1997–2007) on remotely sensed net primary production (NPP) with the iron:carbon (Fe:C) molar ratios for resident phytoplankton to produce Southern Ocean maps of Fe utilization. This approach exploits the resolution of remotely sensed data to investigate the spatial patterns, areal extent and interannual variability of Fe utilization, and relates it to published temporal and spatial trends for Fe supply mechanisms. We estimate that Southern Ocean Fe utilization averaged $\sim 3.3 \pm 0.3 \times 10^8$ mol Fe a^{-1}. This utilization varied little between years (7.8–9.6 μmol Fe m^{-2} a^{-1}), was greatest for subpolar waters, particularly in the Atlantic (up to 53.0 μmol Fe m^{-2} a^{-1}), and was lowest for the polar waters of the Indian sector. Application of maps corresponding to the location and areal extent of Fe supply regions (e.g., dust deposition) revealed that Fe utilization was highest in waters supplied by Patagonian dust, and to a lesser extent, where sediment resuspension (i.e. <500 m depth) probably supplies the majority of the Fe. The Atlantic sector has regions where multiple supply mechanisms are evident, resulting in perennially high productivity. This approach provides a better assessment of the relative importance, realm of influence, and areal extent of different Fe supply mechanisms to Southern Ocean waters.

Citation: Boyd, P. W., K. R. Arrigo, R. Strzepek, and G. L. van Dijken (2012), Mapping phytoplankton iron utilization: Insights into Southern Ocean supply mechanisms, *J. Geophys. Res.*, *117*, C06009, doi:10.1029/2011JC007726.

1. Introduction

[2] Iron (Fe) biogeochemistry has evolved in the last three decades, with an increased focus on studies into both trace metal chemistry and the role of changes in Fe supply in altering the ocean carbon cycle [*Boyd and Ellwood*, 2010]. A central goal of this biogeochemical discipline has been to identify the main sources of Fe to the ocean, with early studies pointing to the key roles of aerosol and upwelled Fe in the High Nitrate Low Chlorophyll (HNLC) waters of the northeast Pacific [*Martin et al.*, 1989] and polar Southern Ocean [*de Baar et al.*, 1995], respectively. There is increasing evidence, from studies of both climate variability and natural perturbations, which document how increased Fe supply, either via upwelling in the Equatorial Pacific [*Chavez et al.*, 1999] or from volcanic eruptions such as in the NE Pacific [*Hamme et al.*, 2010], can have a pronounced effect on oceanic productivity. Hence, a more comprehensive quantification of Fe supply is needed to better understand how Fe biogeochemistry influences patterns of net primary production (NPP).

[3] The HNLC waters of the Southern Ocean have the largest inventory of unused surface macronutrients and have consequently been the focus of six in situ mesoscale Fe-enrichment experiments [*Boyd et al.*, 2007]. In addition, these waters probably have the most diverse range of Fe supply mechanisms in the World Ocean, ranging from aerosol dust and eddy shedding, to sea-ice and iceberg meltwaters [*Lancelot et al.*, 2009; *Boyd and Ellwood*, 2010; *Smith*, 2011]. As a changing climate will probably alter the relative influence of many of these supply terms, a more accurate assessment of their present-day magnitude, areal extent, geographical realm of influence, and interannual variability would be of value to the Southern Ocean biogeochemical modeling community. However, the geographical isolation of these waters makes such an assessment problematic. One approach that has been

[1]NIWA Centre for Chemical and Physical Oceanography, Department of Chemistry, University of Otago, Dunedin, New Zealand.
[2]National Institute of Water and Atmosphere, Greta Point, Wellington, New Zealand.
[3]Environmental Earth System Science, Stanford University, Stanford, California, USA.
[4]Department of Chemistry, University of Otago, Dunedin, New Zealand.

Corresponding author: P. W. Boyd, NIWA Centre for Chemical and Physical Oceanography, Department of Chemistry, University of Otago, Dunedin 9012, New Zealand. (Pboyd@chemistry.otago.ac.nz)

successfully employed in the Southern Ocean to overcome its isolation is that of remote-sensing, which has clearly revealed spatial distributions and temporal trends in chlorophyll [*Sullivan et al.*, 1993] and NPP [*Arrigo et al.*, 2008].

[4] An early and seminal approach to investigate global patterns in phytoplankton Fe utilization was that used by *Fung et al.* [2000] who combined the comprehensive coverage offered by remote-sensing with that of data on phytoplankton iron:carbon (Fe:C) ratios derived from lab culture studies of temperate species [*Sunda and Huntsman*, 1995]. Together, these enabled *Fung et al.* [2000] to map regional patterns in biological Fe requirements for the global ocean and to discuss how such Fe requirements could be met. In the last few years, there has been considerable progress in the development of regionally validated algorithms for satellite remote-sensing products such as NPP, including Arctic waters [*Pabi et al.*, 2008] and the Southern Ocean [*Arrigo et al.*, 2008]. Furthermore, a suite of Fe:C ratios for the resident phytoplankton of the Southern Ocean is now available for both Fe-replete and Fe-deplete conditions [*Twining et al.*, 2004; *Strzepek et al.*, 2011]. Thus, we are now well placed to re-apply the approach of *Fung et al.* [2000] to the Southern Ocean, and to improve upon it, due to recent advances in both regionally validated NPP algorithms and the availability of regional phytoplankton Fe:C ratios.

[5] In the present study, we produced high spatial resolution annual maps of phytoplankton Fe utilization for the Southern Ocean over the period 1997–2007. The maps enable us to tackle several pivotal issues. These include an assessment of the relative contribution of different Southern Ocean zones (ocean basins, or open-ocean ice-free waters versus seasonally ice-covered waters) to phytoplankton Fe utilization; an assessment of the effect of interannual variability on these spatial patterns; and a comparison of these temporal and spatial patterns in Fe utilization with that of known Fe supply mechanisms. Critically, we can compare the magnitude of and spatial trends in phytoplankton Fe utilization with those for current estimates of Fe supply at the ocean basin or biome scale. This enables us to evaluate the relative importance and regional influence of the many Fe supply mechanisms prevalent in these waters.

2. Methods and Materials

2.1. Preamble

[6] To construct maps of phytoplankton Fe utilization for the Southern Ocean required the following steps. First, we obtained the time series of NPP annual composites from 1997 to 2007 for the Southern Ocean presented in *Arrigo et al.* [2008]. Second, we divided the Southern Ocean into regions that were characterized by high Fe/highly productive waters (such as downstream of Kerguelen [see *Blain et al.*, 2007]) versus those which are low Fe/low productivity HNLC waters [*Boyd et al.*, 1999], and also into regions dominated by different phytoplankton functional groups such as diatoms and *Phaeocystis antarctica* [*Arrigo et al.*, 2000]. We then calculated a series of annual composites of phytoplankton Fe utilization by applying the relevant Fe:C molar ratios, derived from either Fe-replete or Fe-deplete phytoplankton species, to NPP for the appropriate region of the Southern Ocean.

2.2. The Southern Ocean NPP Archive

[7] The first stage of developing Fe utilization maps was to carry out further analysis of the annual NPP composites based on the *Arrigo et al.* [2008] NPP algorithm. The archive at present is comprised only of annual composites for 1997–2007. Thus, the first task was to derive a single composite for this period, akin to a standard run in a modeling simulation, which could be in turn related to both interannual trends in phytoplankton Fe utilization and annual Fe supply. The median, rather than the mean, annual NPP for the ten seasons was used because anomalously high production rates at certain locations in some years would have biased the mean in such a short time series, yielding an unrealistic climatological representation.

2.3. Demarcation of the Southern Ocean

[8] In order to use algal Fe:C ratios to transform the NPP median composite to that for phytoplankton Fe utilization, the waters of the Southern Ocean were divided into regions that reflect both the predominance of different algal groups and whether they are generally characterized by high or low Fe concentrations. Based on the availability of Fe:C ratios for different algal groups, we divided the Southern Ocean into three regions dominated by either diatoms, *P. antarctica*, or HNLC phytoplankton (Figure 1a). We assumed that all NPP is accounted for by these three groups, even though there is evidence of other groups contributing to the composition of the phytoplankton assemblage in both subpolar [*Daly et al.*, 2001] and polar [*Twining et al.*, 2004] waters. The Southern Ocean was also divided into Fe-deplete or Fe-replete waters (Figure 1a) using a chlorophyll-based threshold of 1.0 μg L^{-1}, a concentration commonly reported for blooms in polar and subpolar waters [*Blain et al.*, 2007; *Pollard et al.*, 2009; *Moore and Abbott*, 2000; *Smith et al.*, 2000]. One simplification used in our demarcation is that some waters, such as the AESOPS (Antarctic Environment and Southern Ocean Process Study) [*Smith et al.*, 2000] transect northward out of the Ross Sea, have high Fe in early spring prior to a bloom event, and then low Fe thereafter [*Measures and Vink*, 2001; *Sedwick et al.*, 2011]. However, as much of the NPP, and hence Fe utilization, over the growth season takes place over this spring period [*Smith et al.*, 2000] we have designated such regions as high Fe.

2.4. Phytoplankton Fe:C Ratios

[9] The Fe:C molar ratios used to develop the Fe utilization maps were mainly derived from lab cultures from the NIWA Southern Ocean culture collection, Dunedin, New Zealand. Monitoring of their physiological characteristics over the last decade has revealed no evidence of 'physiological drift' imposed by acclimation to lab culture conditions [*Strzepek et al.*, 2011]. Molar ratios for both diatom species and *P. antarctica* were available from steady state cultures under both Fe-replete and Fe-deplete conditions (Tables 1a and 1b) and were assumed to broadly represent, in the context of annual maps of Fe utilization, the influence of the wide range of Southern Ocean dissolved Fe concentrations [*Measures and Vink*, 2001; *Blain et al.*, 2007] and physiological states of phytoplankton (from chlorosis to luxury uptake). The Fe:C ratios obtained for Fe-replete cultures of diatoms and *P. antarctica* were applied to the high Fe waters where these species are dominant, and the ratios from Fe-deplete

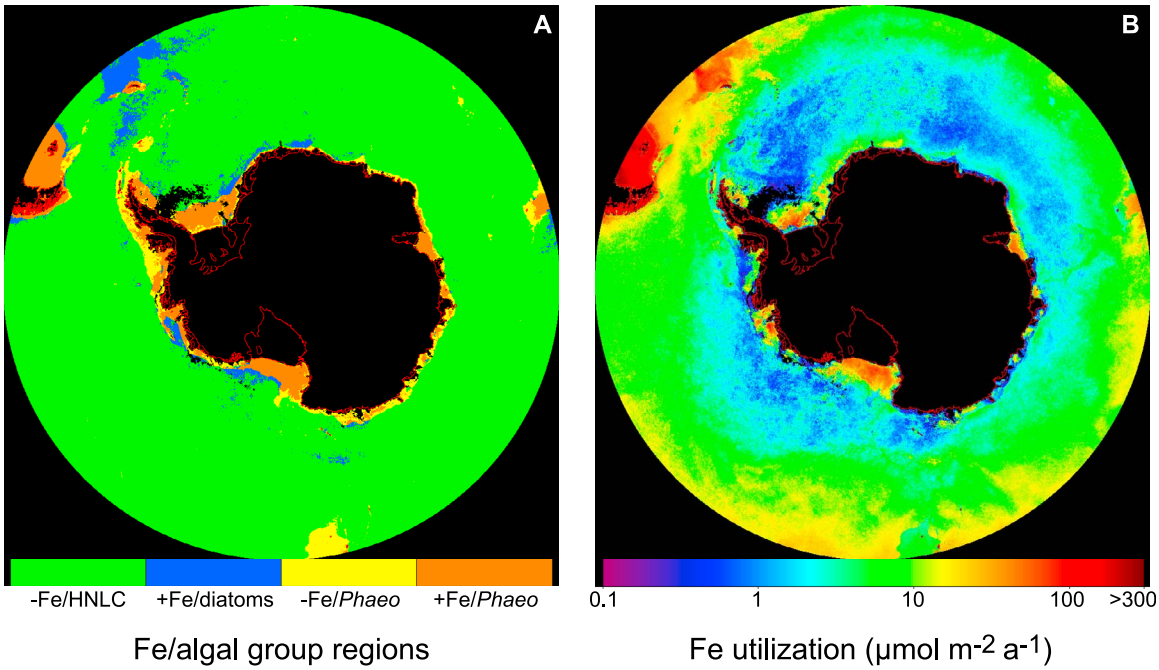

Figure 1. (a) Demarcation of Southern Ocean into regions dominated by different algal groups (i.e., green region denotes low Fe / HNLC waters; blue is high Fe / diatom-dominated waters; yellow is low Fe / *Phaeocystis antarctica*-dominated waters; orange is high Fe / *P. antarctica*-dominated waters for the median composite (referred to as standard run, see main text for more details)). (b) Median composite Fe utilization map (μmol m^{-2} a^{-1}) reprojected with a resolution of around 1 km, with the original NPP estimates being based on SeaWiFS 9 km Level 3 data.

cultures were assigned to low Fe waters where these groups predominate (Figure 1a and Tables 1a and 1b). A generic HNLC phytoplankton community was represented using a mean intracellular Fe:C ratio, derived from Synchrotron X-Ray Fluorescence (SXRF) elemental analysis, for a photosynthetic flagellate and diatom from the HNLC waters at the SOFEX (Southern Ocean Fe Experiment) site south of the Polar Front [*Twining et al.*, 2004]. This ratio was applied to HNLC waters (Figure 1a and Tables 1a and 1b).

2.5. Construction of a Southern Ocean Fe Supply Map

[10] We constructed an Fe supply map in a stepwise manner to compare and contrast with the utilization map. First, estimates of new Fe fluxes from each supply mechanism were collated based on published reports of their estimated geographical location(s), areal extent, temporal signature (i.e., episodic versus sustained), and flux of new Fe (Table 2). Second, because the estimates of phytoplankton Fe utilization represent NPP that is fuelled by both new and regenerated Fe [*Boyd et al.*, 2005; *McKay et al.*, 2005], regional Fe supply was computed using estimates of new Fe supply in conjunction with the regional *f*e ratio (i.e., new Fe/(new + regenerated Fe) [from *Boyd et al.*, 2005]). The *f*e ratios employed were those reported for either low Fe HNLC polar waters (0.1) [*Bowie et al.*, 2009], subpolar waters (0.1) [*Boyd et al.*, 2005; *Bowie et al.*, 2009], or high Fe waters (0.5 (Kerguelen)) [*Sarthou et al.*, 2008].

[11] Several caveats must be considered when constructing such Fe supply maps. First, Fe supply rates were not always available, and so for some supply mechanisms, such as bottom pressure torque [*Sokolov and Rintoul*, 2007], chlorophyll was used as an Fe proxy using Fe:chlorophyll ratios from lab-cultured Southern Ocean phytoplankton (R. F. Strzepek et al., unpublished manuscript, 2012). There are issues with using chlorophyll as a proxy, since Fe:

Table 1a. Phytoplankton Fe:C Molar Ratios Employed for the Standard Run (i.e., Median Composite) and for the Sensitivity Analysis Shown in Figure 12 on Properties Used to Estimate Phytoplankton Iron Utilization From NPP[a]

	Fe:C Ratio		
Algal Groups	Case 3 (mol:mol $\times$ 10^{-6})	Case 2	Case 1
Diatoms/HNLC	Replete 20.0 (deplete 10.0)	12.0 (7.4)	4.0 (5.5)
P. antarctica	Replete 8.6 (deplete 2.3)	8.6 (2.3)	8.6 (2.3)

[a]Range of Fe:C molar ratios assigned to each algal group (upper bound is case 3 (std. run), intermediate ratio is case 2, lower bound is case 1, see Figure 12). All ratios are from lab culture studies [*Strzepek et al.*, 2011] with the exception of the HNLC (Fe-deplete) which is from *Twining et al.* [2004]. *Strzepek et al.* [2011] report 3-fold lower Fe:C ratios for Fe-deplete cells than estimated from field samples by *Twining et al.* [2004]. Note, *Fung et al.* [2000] assigned Fe:C molar ratios of 3.5 $\times$ 10^{-6} to the N part of Southern Ocean and 2.5 $\times$ 10^{-6} to the S waters (see main text for more details).

Table 1b. Alteration of the Areal Extent of Low Fe Southern Ocean Waters When Using Different Chlorophyll Thresholds During the Sensitivity Analysis Shown in Figure 12

Threshold for HNLC waters	Areal extent of HNLC waters (km^2)
<0.3 μg chla L^{-1}	20788412
<0.5 μg chla L^{-1}	36185866
<1.0 μg chla L^{-1} (Std run)	42174438

Table 2. Summary of Published Fluxes of New Fe Supply From a Wide Range of Mechanisms Based on Observations and Modeling Studies[a]

Mechanism	Direct/Indirect/Modeled	Region /Season	Flux (nmol Fe m^{-2} d^{-1})	Extrapolated Flux[b] (μmol Fe m^{-2} a^{-1})	Total Fe Supply[c] (μmol Fe m^{-2} a^{-1})
Island wake (Vertical Fe flux)	DFe and vert diffusivity [*Blain et al.*, 2007]	Kerguelen (HNLC)/Summer	4	0.8	8.0
	DFe and vert diffusivity [*Blain et al.*, 2007]	Kerguelen (Fe-fert)/Summer	31	23.3	46.6
	DFe and Radium isotopes [*Charette et al.*, 2007]	Crozet/Summer	6–31	0.9–23.3	9.0–46.6
Lateral Fe flux from shelf regions	DFe and Radium isotopes [*Charette et al.*, 2007]	Crozet/Summer	64–390	9.8–58.5	19.6–117.0
Atmospheric Fe deposition	Modeled SWAMCO [*Lancelot et al.*, 2009]	S. Atlantic/Patagonia/dust season	43	6.5	
	Modeled SWAMCO [*Lancelot et al.*, 2009]	Coastal Antarctica/Peninsula	1–26	0.2–3.9	0.4–7.8
	Direct measurements [*Wagener et al.*, 2008] linked to depositional model [*Mahowald et al.*, 2005]	Mean values (range of 1–10% Fe solubility) Patagonia; S. Africa; Australia	3.2–51.2; 3.2–51.2; 3.2–51.2	1.1–18.9; 1.1–18.9; 1.1–18.9	11–37.8; 11–37.8; 11–37.8
Ice berg drift and melt	Modeled SWAMCO [*Lancelot et al.*, 2009]	Antarctica/continental shelves	19	2.9	5.8
	Modeled SWAMCO [*Lancelot et al.*, 2009]	N of 60S	0	0	0
	Measured Fe in nanoparticles - extrapolated [*Raiswell et al.*, 2008]	S of 60S Glacial and iceberg supply	NA	54–108[d]	108–216
	Measured Fe in nanoparticles – extrapolated [*Shaw et al.*, 2011]	N Weddell Sea ("Iceberg Alley")	NA	36–363	72–726
Sediment resuspension	Estimated [*Blain et al.*, 2007]	Kerguelen	100	15	30
	Estimated from DFe and Radium isotopes [*Dulaiova et al.*, 2009]	Antarctic Peninsula (Elephant Island)	1800	270	540
	Modeled [*Moore et al.*, 2004]	<1100 m depth	2000	300	600
Seasonal Sea-ice melt	Modeled (based on *Lannuzel et al.* [2007]) by *Lancelot et al.* [2009]	Ross Sea	800	120	240
	Modeled (based on *Lannuzel et al.* [2007]) by *Lancelot et al.* [2009]	Amundsen/Bellingshausen Sea	<10	<1.5	<3
	From seasonal increase in [chlorophyll][e] reported by *Smith et al.* [2000]	AESOPS transects into Ross Sea	na	330	660
Eddy shedding	DFe profiles/modeled eddy dynamics [*Xiu et al.*, 2011]	Gulf of Alaska[f]	>1000	>15	>30
Lateral advection of shelf sediments (and dust)	Tracer release model [*Bowie et al.*, 2009]	East Australia current at N boundary of sub-Antarctic waters	85–191	31–70	62–140
Bottom Pressure Torque (Bathymetric interactions /Upwelling)	Derived from increase in [chlorophyll][g] at circumpolar fronts from *Sokolov and Rintoul* [2007]	Narrow latitudinal bands associated with all circumpolar fronts	33–150	12–55	24–110
Vertical diffusivity	Measured DFe profile and assumed K_z [*Bowie et al.*, 2009]	Polar Front	7	2.5	25
Vertical diffusivity	Measured DFe profiles and K_z from micro-turbulence profiler [*Boyd et al.*, 2005]	Subantarctic waters S of New Zealand	15	5.5	55
Hydrothermal iron supply to upper ocean	Fe biogeochemical and circulation model [*Tagliabue et al.*, 2010; also personal communication, 2012]	Southern Ocean	NA	2–3	4–30[h]

[a]Note each of these supply mechanisms will be altered by varying degrees by climate change. NA denotes not available.

[b]Based on an phytoplankton growth season of 150 days [*Smith et al.*, 2000] except for ocean physical processes such as upwelling, advection and diffusivity which we multiplied by 365.

[c]Total iron is calculated new Fe supply using the 1/*fe* ratio (10 and 2 for HNLC and high Fe waters, respectively). In some cases the Fe status of the waters was assigned arbitrarily due to the paucity of data coverage for dissolved Fe [*Boyd and Ellwood*, 2010].

[d]Denotes estimated using bioavailable Fe fluxes (expressed in Tg a^{-1}) divided by areal extent of waters S of 60S from *Raiswell et al.* [2008].

[e]Converted to Fe flux using Fe:chlorophyll ratios (for Fe-replete polar diatoms (R. F. Strezepek unpublished data, 2012)) based on an increase of ~1.0 μg L^{-1} chlorophyll over background levels.

[f]In lieu of such detailed estimates from the S. Ocean.

[g]Converted to Fe flux using Fe:chlorophyll ratios (for Fe-replete polar diatoms (R. F. Strezepek unpublished data, 2012)) and an increase of ~0.1 or ~0.2 μg L^{-1} chlorophyll over background HNLC values (~0.3 μg L^{-1}) reported in *Sokolov and Rintoul* [2007].

[h]Hydrothermal Fe will add to the inventories of both low and high Fe waters (hence *fe* ratios from both regions were used to set lower and upper bounds).

Table 3. Temporal Variability in Fe Supply Mechanisms[a]

Mechanism	Region	Duration	Interannual Variability	Method
Atmospheric Fe deposition	Australia *Mackie et al.* [2008]	50 year study	8-fold	Dust Visibility Reduction
	S. Atlantic/Patagonia *Gaiero et al.* [2003]	1 year study	5 fold between seasons	Dust fluxes
Ice berg drift and melt	Weddell Sea *Schodlok et al.* [2006]	5 year study	Variable drift patterns (see Figure 2 in *Schodlok et al.*) 2-fold based on iron utilization map for icebergs (see Figure 10d)	Microwave remote sensing
Seasonal Sea-ice melt	MIZ *Stammerjohn et al.* [2008]	10 year study	<2 fold (i.e., 1.1 to 1.5 × 10^7 km^2 (see Figure S1 in Text S2 of the auxiliary material))	Microwave remote sensing

[a]For an estimate of the areal extent of each Fe supply term see iron utilization maps in Figure 11. For most of the supply mechanisms presented in Table 2 there is no published information on interannual variability.

chlorophyll ratios change depending on phytoplankton physiology (R. F. Strzepek et al., unpublished manuscript, 2012). Second, care must be taken when comparing estimates of Fe supply that are based on mechanisms that range from sustained (i.e., year-round such as hydrothermal supply [*Adams et al.*, 2011]) to episodic (i.e., days, for example bushfires [*Boyd et al.*, 2010]) with Fe utilization derived from annual estimates. To address this potential mismatch, we specifically compared Fe supply from mechanisms evident over timescales of a month or greater.

[12] The temporal resolution of the Fe supply map is much poorer than that for the satellite- derived utilization maps. In order to assess how the interannual variability in Fe utilization compared with that for Fe supply, we used estimates of interannual variability in specific supply mechanisms, such as dust variability [*Gaiero et al.*, 2003] and sea-ice retreat [*Stammerjohn et al.*, 2008] (Table 3). In some cases, no data on the interannual variability of Fe supply mechanisms were available. This issue was addressed by assessing the interannual variability in Fe utilization for specific regions in which distinct Fe supply mechanisms are reported to be dominant, for example the resuspended sedimentary Fe map for waters <500 m depth (see section 2.6).

2.6. Construction of Regional Fe Utilization maps

[13] To explore in detail the relationship between phytoplankton Fe utilization and Fe supply, a map of Fe utilization was created for each biogeochemical Fe supply mechanism that had both a well characterized geographical location and was of sufficient areal extent. For example, maps of Fe utilization were constructed for aerosol Fe supply from each of the three main dust source regions – Patagonia, South Africa and Australia [*Jickells et al.*, 2005]. However, for other Fe supply mechanisms – such as bottom pressure torque [*Sokolov and Rintoul*, 2007] – it was not possible to produce a map of Fe utilization that corresponded to each of the relatively narrow and meandering circumpolar bands. The areal extent of several Fe supply mechanisms was estimated indirectly from Fe utilization maps (see section 2.7).

[14] The bounds for the aerosol Fe maps from Patagonia, South Africa, and Australia are based on the map presented in *Wagener et al.* [2008] using a revised version of a *Mahowald et al.* [2005] dust model. The modeling study of *Moore and Braucher* [2008] also provided useful guidelines for using bathymetric maps (using either a 500 m or 1000 m depth threshold) to assess patterns in Fe utilization in regions where resuspended sedimentary Fe is prevalent. The maps for seasonal sea-ice melt, and iceberg drift and melt are based on the time series of sea-ice retreat presented in *Stammerjohn et al.* [2008] and from a detailed analysis (using microwave scatterometry) of iceberg drift trajectories from "Iceberg Alley" in the North Weddell Sea by *Stuart and Long* [2011], respectively. To enable comparison with the Fe supply maps, each regional Fe utilization map was expressed in units of μmol Fe m^{-2} a^{-1}. The maps were used in three ways. First, to compare the magnitude of, and patterns in, Fe supply and utilization for specific regions. Second, to assess the potential heterogeneity of Fe utilization (and hence supply) from processes such as sea-ice melt that are thought to vary widely between regions [*Lancelot et al.*, 2009]. Third, to examine how the lateral Fe utilization (and hence supply) from resuspended sediments might be attenuated with distance by comparing observations from the Antarctic Peninsula ((Atlantic sector) [*Dulaiova et al.*, 2009; *Ardelan et al.*, 2010]) with the sedimentary Fe maps.

2.7. Fe Utilization: Sensitivity Analysis

[15] Additional comparisons between the magnitude of phytoplankton Fe utilization and Fe supply were made by conducting sensitivity analyses to explore the effect of altering the threshold (expressed as chlorophyll concentration) used to demarcate Fe-replete versus Fe-deplete waters, and of applying different algal Fe:C ratios (Tables 1a and 1b), as a wide range of values have been reported for lab cultures [*Sarthou et al.*, 2005; *Strzepek et al.*, 2011] and there are threefold differences between lab-culture estimates [*Strzepek et al.*, 2011] and those from the field [*Twining et al.*, 2004] for iron deplete cells (Tables 1a and 1b). Another factor inherently considered in the comparison of total Fe supply with that of algal Fe utilization is that of the Fe supplied to other biological components of the pelagic food web [*Boyd and Ellwood*, 2010].

3. Results

3.1. Trends in Phytoplankton Fe Utilization

[16] The median composite of Fe utilization for the period 1996–2007 reveals a variegated Southern Ocean in which there are both meridional and zonal gradients and distinct inter-basin and regional (i.e., ice-free waters versus seasonally ice-covered) trends (Figure 1b). The regions of highest Fe utilization are clearly evident east of Patagonia on the Malvinas/Falklands continental shelf and eastward into the subpolar Atlantic waters. Other regions of high Fe utilization are close to Antarctica, for example in the Ross and Weddell Seas, and downstream (i.e., eastward) from offshore islands

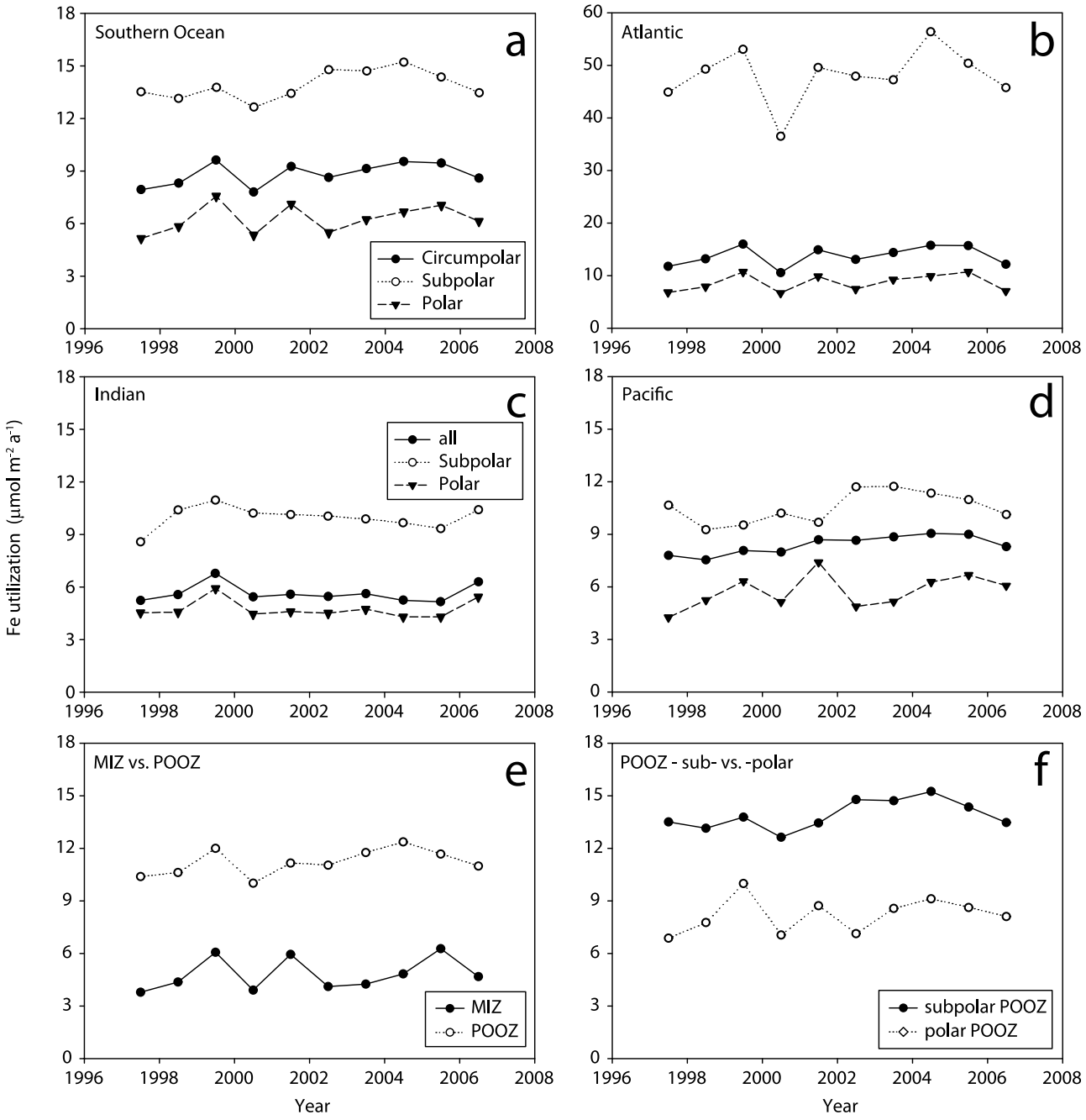

Figure 2. Phytoplankton Fe utilization per unit area (μmol m^{-2} a^{-1}) for (a) circumpolar Southern Ocean; (b) Atlantic basin; (c) Indian basin; (d) Pacific basin; (e) MIZ versus POOZ; (f) POOZ subpolar versus polar waters.

such as South Georgia (Atlantic Ocean sector) and Kerguelen (Indian Ocean sector, Figure 1b). The Atlantic sector has the greatest Fe utilization per unit area and there is generally a poleward decrease in Fe utilization from subpolar waters toward coastal Antarctica.

[17] These initial observations are confirmed by the Fe utilization (μmol m^{-2} a^{-1}) for subpolar waters north of the Polar Front that is ~2-fold higher than in polar waters (Figure 2a). Furthermore, this trend is particularly pronounced in the Atlantic sector where subpolar waters have a ~5-fold higher phytoplankton Fe utilization than in polar waters (Figure 2b). Both the Indian and Pacific sectors have a ~2-fold greater utilization for Fe in subpolar waters relative to those south of the Polar Front (Figures 2c and 2d). The Atlantic sector (polar and subpolar) has the highest utilization for Fe, on a unit area basis, followed by the Pacific, and then the Indian sectors (Figures 2b–2d). A comparison of the Fe utilization of phytoplankton in the Permanently Open Ocean Zone (POOZ) [*Tréguer and Jacques*, 1992] versus that for the Marginal Ice Zone (MIZ) [*Tréguer and Jacques*, 1992] reveals that the POOZ has a ~2-fold greater Fe utilization than the MIZ (Figure 2e). When the POOZ is subdivided

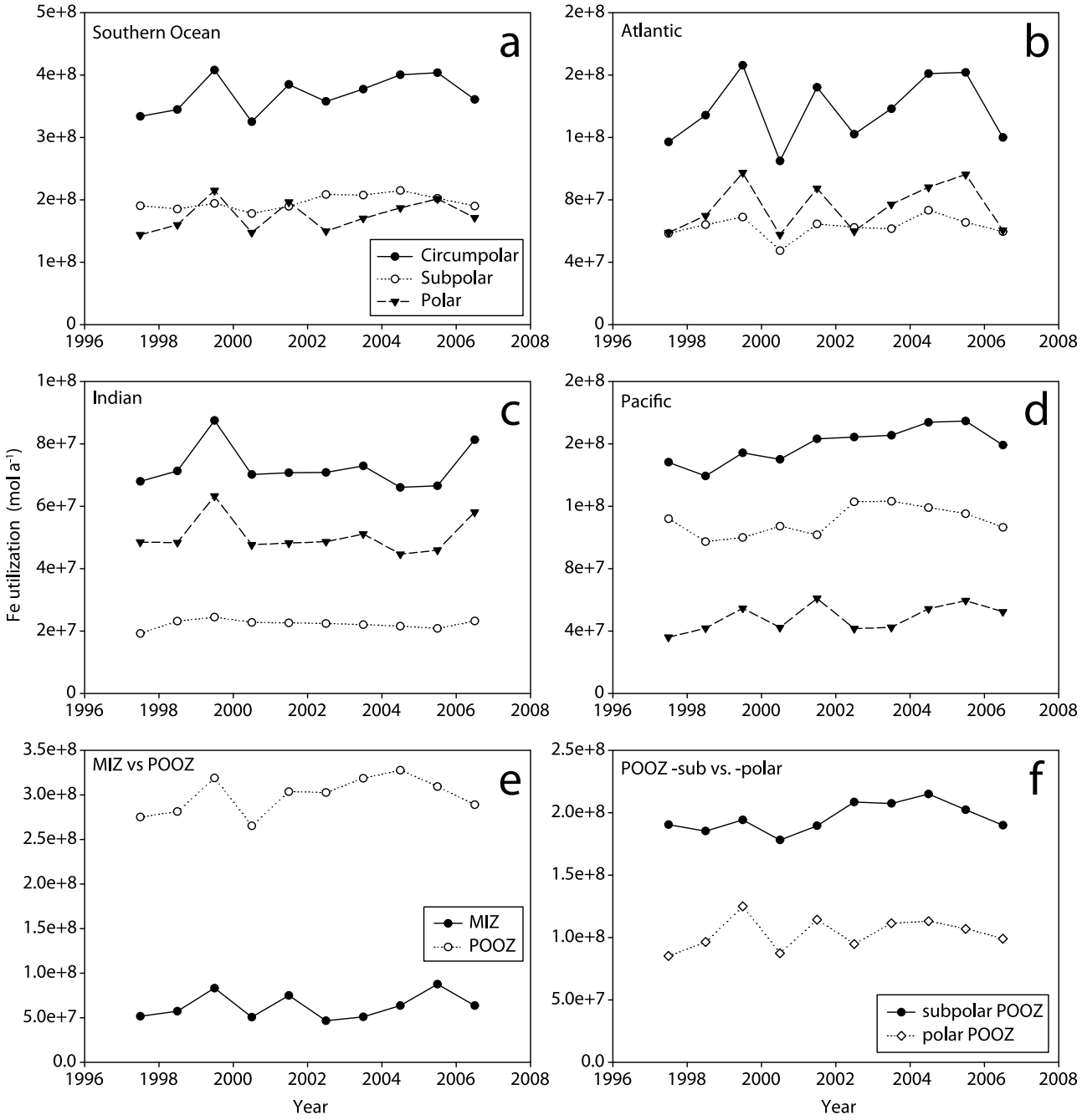

Figure 3. Phytoplankton Fe utilization (mol a^{-1}) for (a) circumpolar Southern Ocean; (b) Atlantic basin; (c) Indian basin; (d) Pacific basin; (e) MIZ versus POOZ; (f) POOZ subpolar versus polar.

into subpolar and polar regions, as for the Southern Ocean basins, the subpolar waters have a consistently higher Fe utilization (~1.5-fold, Figure 2f).

[18] The areal extent of each basin and region shown in Figure 2 are provided in Tables S1 and S2 in Text S1 of the auxiliary material and enable the calculation of the absolute Fe utilization (i.e., Fe utilization per unit area x areal extent) for each region.[1] As polar waters comprise most of the Southern Ocean, their areal extent compensates for the lower Fe utilization per unit area south of the Polar Front, and thus the phytoplankton Fe utilization for both subpolar and polar waters are comparable at ~1.5 to 2 × 10^8 mol a^{-1} (Figure 3a). The areal extent of the Pacific, Indian, and Atlantic sectors is 1.9, 1.3, and 1.0 × 10^7 km^2, respectively (Tables S1 and S2 in Text S1 of the auxiliary material). The Pacific sector is the largest contributor to Southern Ocean Fe utilization (Figure 3b), followed by the Atlantic sector, which although is the smallest in areal extent, has a higher per unit area Fe utilization than the Indian sector (Figure 2 c.f. Figure 3). Each sector exhibits different trends in the relative importance of subpolar versus polar

[1]Auxiliary materials are available in the HTML. doi:10.1029/2011JC007726.

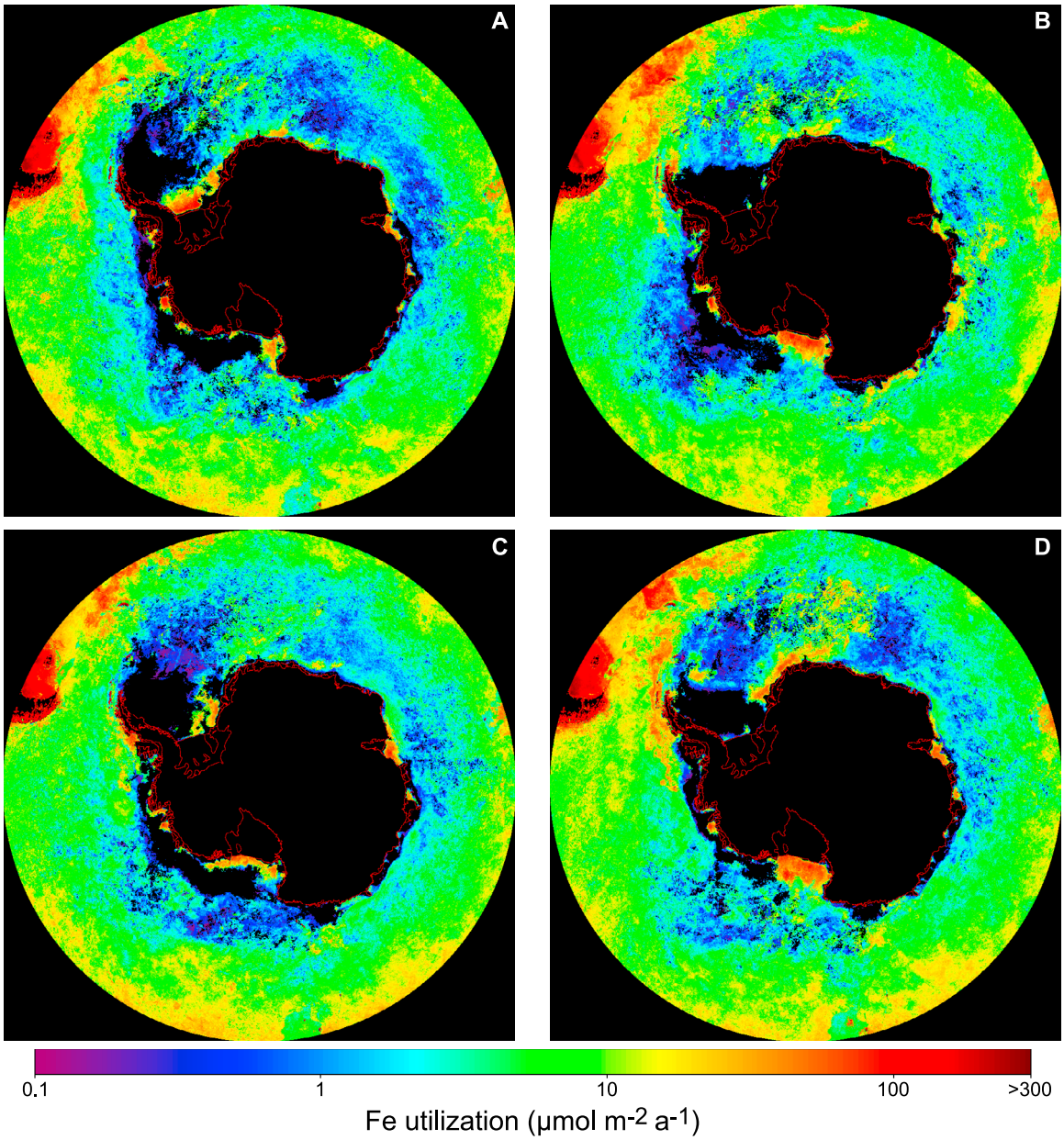

Figure 4. Examples of circumpolar Fe utilization maps from contrasting years with conspicuous regional differences in Fe utilization (see text for more details): (a) 1997; (b) 1999; (c) 2000; (d) 2005.

Fe utilization. In the Atlantic, both regions make a similar contribution, whereas subpolar Fe utilization is significantly higher in the Pacific sector, but the opposite is the case for the Indian sector (Figures 3b–3d). Consideration of the areal extent of the POOZ and MIZ results in the POOZ having a fourfold greater Fe utilization than the MIZ (Figure 3e).

3.2. Interannual Variability in Phytoplankton Fe Utilization

[19] The variability in phytoplankton Fe utilization for the entire Southern Ocean over the period 1996 to 2007 was relatively small whether expressed per unit area (7.8 to 9.6 μmol Fe m^{-2} a^{-1}; standard deviation 0.66 (n-1 = 9)) or in absolute terms (3.3×10^8 to 4.1×10^8 mol a^{-1} (standard deviation 0.3×10^8 (n-1 = 9)). Low interannual variability was also evident when Fe utilization per unit area was expressed at the regional and basin scale, with low variability generally for both subpolar and polar waters for each basin, and for the MIZ versus the POOZ (Figure 2). In some cases, there is evidence of conspicuous anomalies in the time series, such as elevated Fe utilization in a particular year, such as 1999 (circumpolar waters (Figure 2a); Indian sector (Figure 2c), MIZ and POOZ (Figure 2e)), or decreased Fe utilization in 2001 (Atlantic subpolar waters, Figure 2b) that warrant further scrutiny to determine their underlying cause (Figure 4).

[20] Phytoplankton Fe utilization, when expressed as absolute rates, generally exhibited little interannual variability at the basin or regional scale, in particular for subpolar waters (Figures 3a–3d). The Pacific sector exhibited

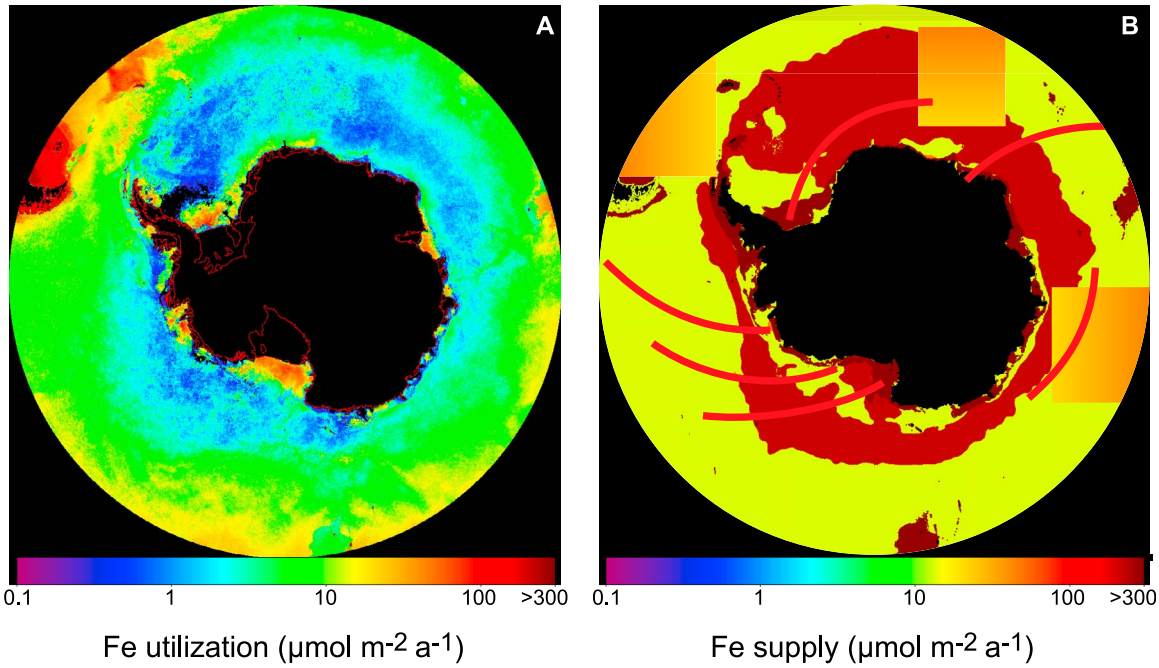

Figure 5. Contrasting maps of (a) Fe utilization (from Figure 1b) and (b) Fe supply (μmol m^{-2} a^{-1}) for the main mechanisms i.e., of large areal extent (from Table 2, for vertical diffusivity (all sea-ice free waters); dust (three regional maps, off Patagonia, S. Africa, Australia, see Figure 6a); icebergs (generic trajectories represented by lines; *Raiswell et al.* [2008], mean value); sea-ice (regional map (see Figure 6c); Ross Sea, *Lancelot et al.*[2009]); sedimentary (see Figure 6b, set to upper limit of scale –300 μmol m^{-2} a^{-1})). Note the Fe supply map is of low resolution and thus is mainly illustrative.

the least interannual variability whereas the Atlantic sector had the greatest, due mainly to that exhibited by polar waters (Figure 3d). The highest circumpolar Fe utilization was in 1999 (Figure 4b), and was probably driven by enhanced utilization in both Indian and Atlantic polar waters (Figures 3c and 3d). These cases were further assessed to determine their underlying mechanisms (Figure 4). For example, a comparison of 1997 with 1999 reveals enhanced Fe utilization in the Atlantic and Indian sectors, downstream of Patagonia, and offshore from the Antarctic ice shelves, respectively (Figures 4a and 4b). In contrast, other regions, including those with waters <1000 m depth, such as around Kerguelen or the Campbell Plateau (south of New Zealand), exhibited low interannual variability in Fe utilization (Figure 4). These differing degrees of interannual variability may provide insights into whether changes in regional Fe supply are enhancing or reducing overall Fe utilization between years.

3.3. Fe Supply

[21] The Southern Ocean is characterized by >10 distinct Fe supply mechanisms that are summarized in Table 2. These mechanisms have different sources (atmosphere, cryosphere, hydrosphere), rates of supply (episodic dust storms, seasonal sea-ice retreat, persistent hydrothermal vent activity), and spatial extent (discrete hydrothermal vents and widespread vertical diffusivity). In addition to supplying Fe, some of these mechanisms also alter other environmental properties such as buoyancy (sea-ice retreat), Fe-binding ligands (hydrothermal), and nutrient supply (upwelling). Together, these factors largely determine the spatial and temporal patterns in phytoplankton Fe utilization for the Southern Ocean (Figures 1b and 4). Given the uncertainties that exist for the areal extent and sphere of influence for each supply mechanism, we have expressed Fe supply on a per unit area basis, the most common manner in which Fe supply is reported.

[22] Estimates of Fe supply in Table 2 are from a range of approaches such as modeling (when observations are sparse, e.g., hydrothermal supply [*Tagliabue et al.*, 2010] or sea-ice melt [*Lancelot et al.*, 2009]), direct observations [*Blain et al.*, 2007], and indirect estimates (for some supply mechanisms such as bottom pressure torque [*Sokolov and Rintoul*, 2007]). Fluxes of new Fe range from ~3 μmol Fe m^{-2} a^{-1} for vertical diffusive supply, which characterizes much of the HNLC POOZ waters, to 300 μmol Fe m^{-2} a^{-1} (at source) for Fe from sediment resuspension in waters of <1000 m depth based on the model of *Moore et al.* [2004]. Other mechanisms had intermediate supply rates ranging from 10 to 50 μmol Fe m^{-2} a^{-1}, including eddy-derived supply, island wakes, bottom pressure torque, and iceberg drift and melt (Table 2). To compare the magnitude of Fe supply and utilization, these supply rates of new Fe were multiplied by 1/*f*e ratio.

3.4. Comparing Fe Supply and Utilization

[23] We first compared the magnitude of total Fe supply (i.e., new and recycled Fe) by each mechanism with the range of estimated phytoplankton Fe utilization (Figure 5). Next, the magnitude of total Fe supply from specific locales, such as Southern Ocean islands like Kerguelen with Fe-island

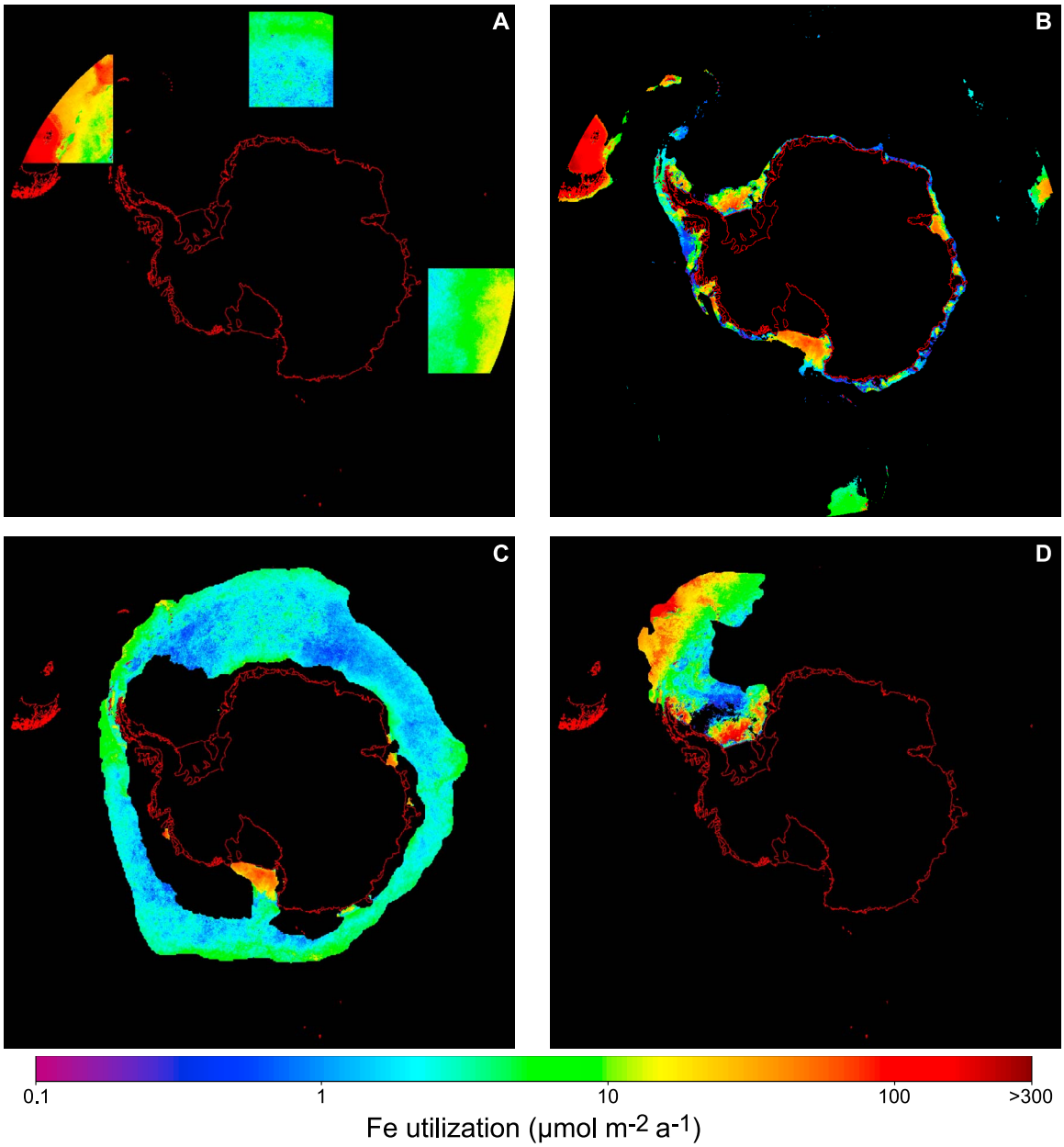

Figure 6. Examples of Fe utilization maps (μmol m^{-2} a^{-1}) for regions in which Fe supply mechanisms are of large areal extent and their geographical locations are well established: (a) dust source regions; (b) bathymetry (<1000 m depth); (c) sea-ice extent; (d) ice-berg drift and melt in the northern Weddell Sea.

wakes [*Blain et al.*, 2007] was compared with the Fe utilization for these locales. In section 3.5, a further level of detail, the consideration of the areal extent of Fe supply mechanisms, was added to this comparison.

[24] Total Fe supply ranged from 10 to 600 μmol Fe m^{-2} a^{-1} (Table 2 and Figure 5) and provides upper and lower bounds on the magnitude of Fe utilization. The upper bound was associated with nearshore waters of <1000 m depth whereas the lower bound was mainly observed in HNLC POOZ waters. These are of the same order as upper and lower bounds of phytoplankton Fe utilization of >100 μmol Fe m^{-2} a^{-1} on the Falklands/Malvinas shelf and close to Antarctica in the Weddell Sea, to <10 μmol Fe m^{-2} a^{-1} in the POOZ surrounding Antarctica (Figure 1b). Near Kerguelen, estimates of vertical Fe supply [*Blain et al.*, 2007] and associated Fe recycling [*Sarthou et al.*, 2008] give an estimate of Fe supply of 45 μmol Fe m^{-2} a^{-1} (Table 2), which compares well with the corresponding phytoplankton utilization of ~30 μmol Fe m^{-2} a^{-1} (Figure 1b). Thus, from this initial comparison, the upper, intermediate, and lower bounds of Fe supply appear to be comparable to that for phytoplankton Fe utilization.

3.5. Comparing Geographical Patterns of Fe Utilization and Supply

[25] The Fe supply rates in Table 2 represent four main mechanisms, a) localized supply that may be constant over a

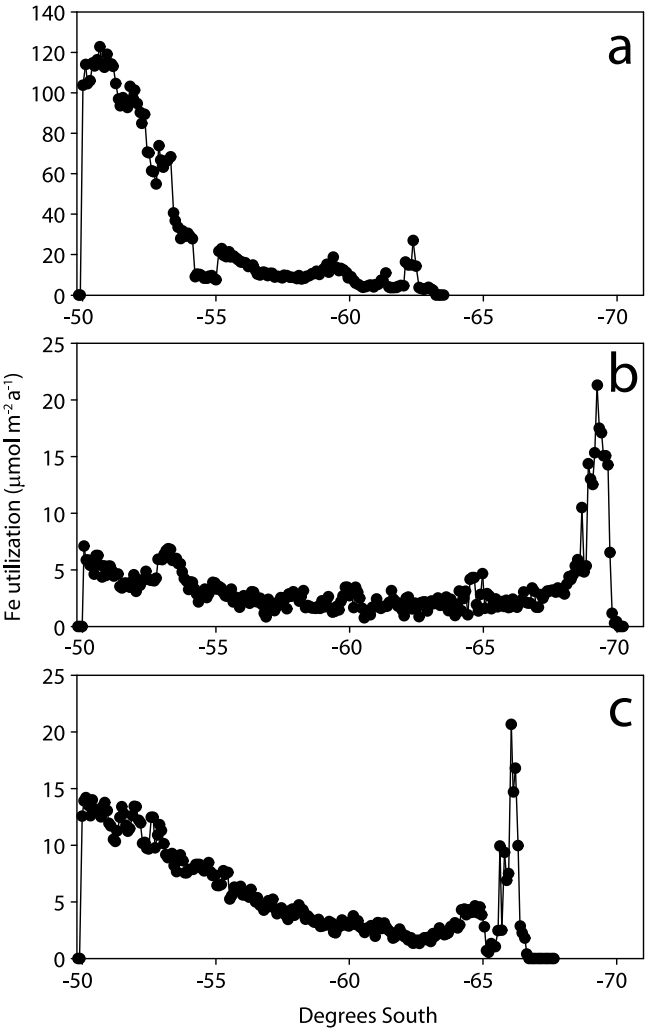

Figure 7. Fe utilization versus distance southwards through each of the dust maps presented in Figure 6a for (a) Patagonia (along the 57.1°W meridian); (b) South Africa (6.9°E meridian) and (c) Australia (108.4°E meridian). Note pronounced 1/2 decrease distance for aerosol iron of <300 km but for Patagonia only.

large area (sea-ice melt, vertical diffusivity), b) point source/regional supply that dissipates with transport (either atmospheric transport from arid/semi-arid regions, *Mackie et al.* [2008] or oceanic such as eddy transport of deep ocean Fe such as from vents [*Adams et al.*, 2011]), c) localized supply over a relatively narrow band (bottom pressure torque and circumpolar fronts [*Sokolov and Rintoul*, 2007]), and d) circumpolar sources that dissipate with lateral transport – sediment resuspension [*Moore and Braucher*, 2008]. Fe supply mechanisms in categories a), b), and d) are probably most readily scaled up to an Fe supply region of significant areal extent. To date, more effort has gone into understanding the patterns and mechanisms of dispersal and deposition of aerosol Fe [*Prospero et al.*, 1989; *Mahowald et al.*, 2005] than is the case for point sources of Fe such as hydrothermal vents [*Tagliabue et al.*, 2010] or resuspended sediments [*Moore and Braucher*, 2008].

[26] Fe utilization from each of the aerosol Fe maps reveals that nearshore rates for Patagonia (where there is also a sedimentary Fe component, see later) were >100 μmol Fe m^{-2} a^{-1}, decreasing offshore to <5 μmol Fe m^{-2} a^{-1} (Figures 6a and 7a). The attenuation of Fe utilization as would be expected in a dust supply region – termed '1/2 decrease distance' i.e., over which 1/2 of the dust load is deposited [*Prospero et al.*, 1989] - was most evident south of Patagonia toward the tip of the Antarctic Peninsula, whereas it was less evident east of Patagonia (Figure 6a), suggesting that other supply mechanisms influence Fe utilization. These utilization rates (Figure 7a) are comparable to aerosol Fe dust fluxes from *Wagener et al.* [2008] of 20 μmol Fe m^{-2} a^{-1} attenuating to ~1 μmol Fe m^{-2} a^{-1} (1% Fe solubility) and ~200 μmol Fe m^{-2} a^{-1} attenuating to ~10 μmol Fe m^{-2} a^{-1} (10% Fe solubility). Lower rates of Fe utilization were evident near South Africa and Australia, and there was evidence of attenuation of Fe utilization with distance from the dust source region across each map (Figures 6a, 7b, and 7c). *Wagener et al.* [2008] reported aerosol Fe fluxes for both regions of ~1 μmol Fe m^{-2} a^{-1} attenuating to 0.2 μmol Fe m^{-2} a^{-1} (1% Fe solubility) and >10 μmol Fe m^{-2} a^{-1} attenuating to ~2 μmol Fe m^{-2} a^{-1} (10% Fe solubility), respectively. Thus, the supply rates based on a solubility intermediate between 1% and 10% were comparable to those from phytoplankton Fe utilization, further supporting the current view that Fe solubility of dust lies between 1% and 10% [*Baker and Croot*, 2010].

[27] The modeling study of *Lancelot et al.* [2009] collated data on Fe supply resulting from sea-ice melt and retreat which suggest that Fe supply varied considerably between regions, from >100 μmol Fe m^{-2} a^{-1} for the Ross Sea to <2 μmol Fe m^{-2} a^{-1} for the Amundsen and Bellingshausen Seas (Table 2). A similar trend is evident for phytoplankton Fe utilization (Figures 6c and 8) with rates higher in the Ross Sea (>60 μmol Fe m^{-2} a^{-1}) than in the Amundsen and Bellingshausen Seas (~10 μmol Fe m^{-2} a^{-1}). Furthermore, the sea-ice Fe utilization map provides indirect evidence of the heterogeneity of Fe supply from sea-ice, ranging from regions that may support a high Fe utilization (Ross and Weddell Sea) to those such as east Antarctica that support much lower Fe utilization (Figure 6c).

[28] The Fe utilization maps reveal how the lateral supply from resuspended sediments might be attenuated with distance (Figures 6b and 9). Consideration of the bathymetric map (Figure 6b) reveal the Fe utilization in regions adjacent to those of <1000 m depth (Figures 9c and 9d), and hence how they may respond to resuspended Fe supply. *Dulaiova et al.* [2009] report that for a phytoplankton bloom north of Elephant Island covering an area of 62500 km^2, a supply of >600 μmol Fe m^{-2} a^{-1} is required. Phytoplankton Fe utilization of ~50 μmol Fe m^{-2} a^{-1} was evident close to the offshore boundary of the 1000 m depth waters (Figures 6b and 9). It is also evident from this map that the lateral attenuation of Fe utilization is rapid (i.e., a 1/2 decrease distance [*sensu Prospero et al.*, 1989] of <300 km) suggesting relatively fast uptake and/or abiotic removal of this Fe, both along Drakes Passage and the west Antarctica Peninsula, before it is transported to offshore waters (Figure 9).

[29] Data sets from the Fe utilization map for iceberg drift and melt (Figure 6d) reveal that the Fe utilization in the vicinity of "Iceberg Alley" varies along a ~4000 km transect

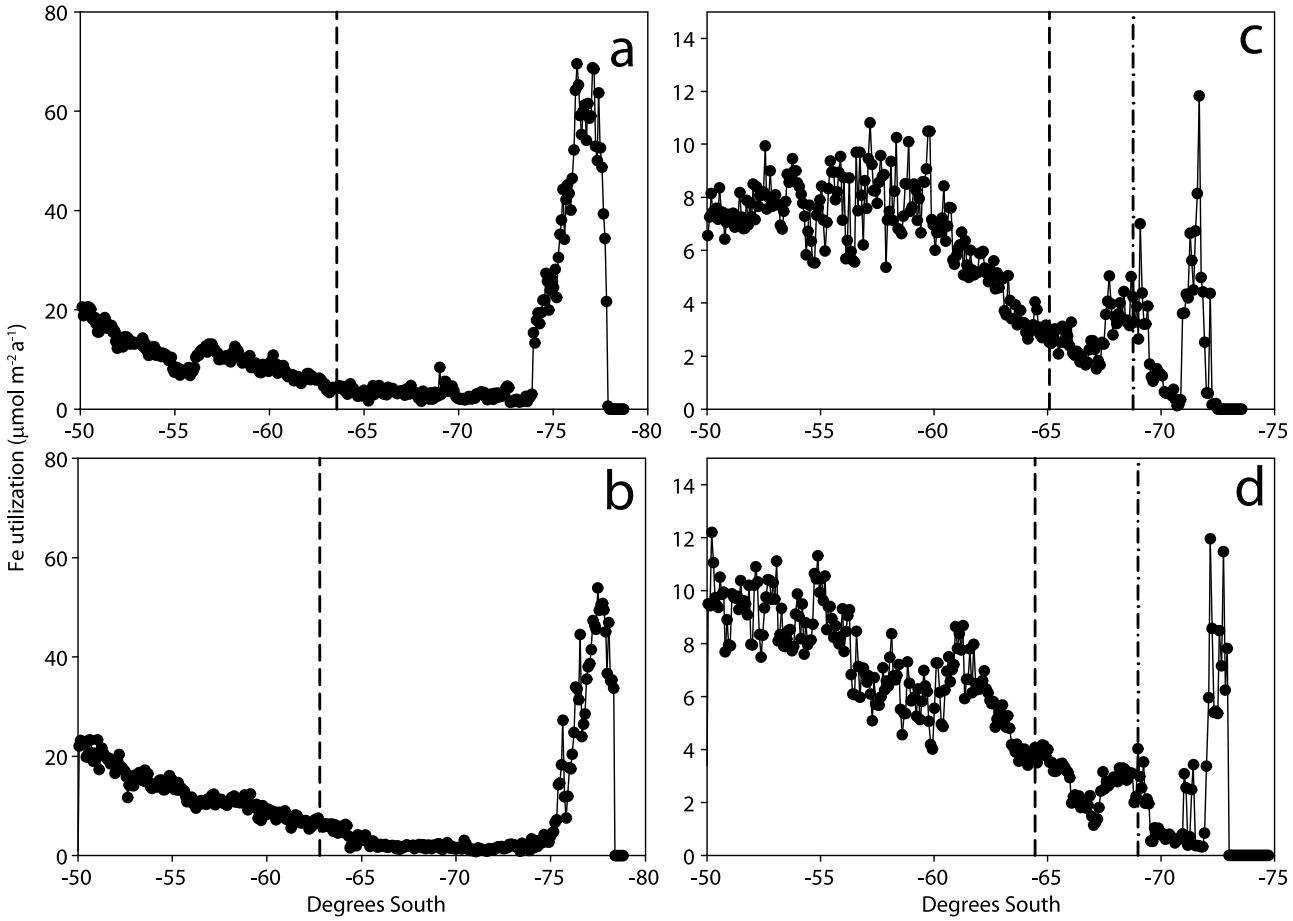

Figure 8. Fe utilization versus distance southwards through the sea-ice retreat map presented in Figure 6c for (a) Ross Sea (180°W meridian); (b) Ross Sea (170°W meridian); (c) Bellingshausen Sea (90°W meridian); and (d) Bellingshausen Sea (80°W meridian). The dashed vertical line denotes the seaward extent of the MIZ (i.e., open water in January but ice in September, see blue region in Figure S1 in Text S2 of the auxiliary material), and the dot-dashed line in Figures 8c and 8d represents the landward extent of the MIZ, i.e., ice for both January and September. (See yellow region in Figure S1 in Text S2 of the auxiliary material).

as the icebergs drift northward out of the Weddell Sea (Figure S2 in Text S2 of the auxiliary material). The rates of iron utilization appear to be considerably less than that potentially supplied from iceberg melt (Figure 6d c.f. Table 2) suggesting some temporal mismatches between supply and utilization. However, determining the extent to which Fe utilization in this region is met by icebergs is not possible due to the confounding effects of overlap with other Fe supply mechanisms such as Patagonian dust and resuspension of shallow sediments (Figure 6).

[30] Taken together, these maps also provide insights into how much areal overlap exists between the spatial realm of influence for different supply mechanisms (Figure 6 and Table S3 in Text S1 of the auxiliary material). For example, there is a 22% overlap between the <1000 m sedimentary Fe and the aerosol Fe map off Patagonia whereas there is virtually no overlap between these supply mechanisms south of Africa or Australia (Table S3 in Text S1 of the auxiliary material). Such overlap may explain the complex patterns in Fe utilization evident within the Patagonian dust map (Figure 6a), which is probably due to Fe being supplied from both sediment resuspension and Patagonian dust. Other areas of overlap between different supply mechanisms include sea-ice melt and sediment resuspension where a 45% overlap of sea-ice melt and resuspension is evident (Figure 6 and Table S3 in Text S1 of the auxiliary material). Some more highly resolved temporal maps of Fe utilization might help tease apart supply mechanisms that have different degrees of seasonality.

[31] The maps also inform debate over the relative contribution of each supply mechanism to total Fe utilization. The Patagonian shelf has the highest Fe utilization per unit area ($\sim$90 μmol Fe m^{-2} a^{-1}), followed by that of the Patagonian aerosol Fe supply (Figures 10a and 10b). In contrast, the South African aerosol Fe and New Zealand sedimentary Fe have the lowest Fe utilization per unit area (Figures 10a and 10b). The Fe utilization in waters influenced by the highest population of drifting icebergs (Figure 6d) had an intermediate value of $\sim$10 μmol Fe m^{-2} a^{-1} (Figure 10d) versus that of $\sim$4 μmol Fe m^{-2} a^{-1} for the MIZ (Figure 10c). In terms of absolute Fe utilization for the area represented by each map, Patagonian dust

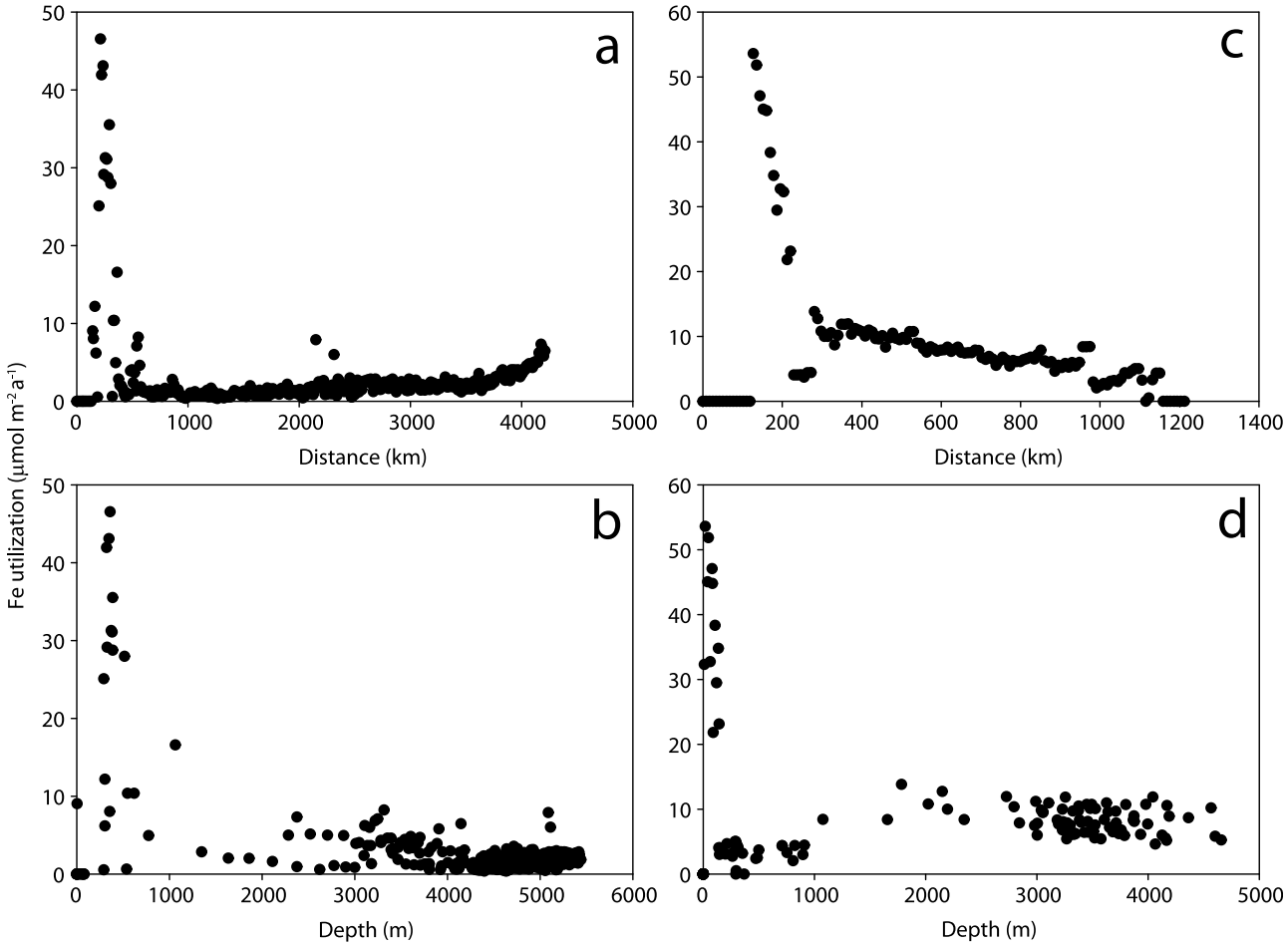

Figure 9. Fe utilization versus distance southwards, or depth, through the sediment resuspension map presented in Figure 6b for (a and b) downstream of shelf iron source in the Western Antarctic Peninsula; (c and d) for Drakes Passage.

has the largest Fe utilization ($\sim 6 \times 10^7$ mol a^{-1}) followed by the Patagonian shelf and MIZ ($\sim 5 \times 10^7$ mol a^{-1}) (Figure 11). In contrast, there was relatively low absolute Fe utilization for sedimentary Fe on the New Zealand shelf/slope waters (Figure 11b).

3.6. Sensitivity Analysis on Factors Influencing Phytoplankton Fe Utilization

[32] The suite of comparisons – from circumpolar to regional - of Fe utilization and supply reveal that both the magnitude of the fluxes and some of the spatial trends are comparable. However, estimates of phytoplankton Fe utilization are sensitive to both the set of Fe:C ratios employed and the threshold for the selection of Fe:C ratios from Fe-replete versus Fe-deplete conditions. Sensitivity analysis reveals that the Fe utilization maps change considerably when each of the three different sets of Fe:C ratios presented in Tables 1a and 1b are selected (Figure 12 and Figure S3 in Text S2 of the auxiliary material). The sensitivity of Fe utilization estimates to altering either Fe:C ratio or the threshold Fe concentration (i.e., the areal extent of HNLC waters and of the dominant phytoplankton groups) is greater for the former (Figure 12), with changes in the magnitude of Fe utilization increasing, relative to the standard run, by ~twofold, depending on what set of Fe:C ratios was employed. In contrast, changing the chlorophyll threshold (i.e., altering the areal extent of HNLC waters by up to twofold, Table 1b) increases the amplitude of algal iron utilization between the three Fe:C cases, with the largest increase (~50%) evident for case 1 (Figure 12). The comparison of phytoplankton Fe utilization with supply should result in an underestimation of biological Fe utilization, as other parts of the microbial and metazoan communities also have Fe requirements [*Boyd and Ellwood*, 2010]. Detailed Fe biogeochemical budgets of Southern Ocean waters reveal that phytoplankton account for ~60% of community Fe utilization for low Fe waters, whereas in high Fe waters (Kerguelen), they make up <50% [*Boyd and Ellwood*, 2010]. Thus, estimates of biological Fe utilization can vary by several-fold depending on the selection of Fe:C ratios, HNLC threshold, and on the inclusion of part or all of the biological Fe utilization.

4. Discussion

4.1. Comparison With a Prior Estimate of Fe Utilization

[33] Our Southern Ocean circumpolar estimate of phytoplankton Fe utilization of $\sim 4 \times 10^8$ mol a^{-1} is 30-fold less

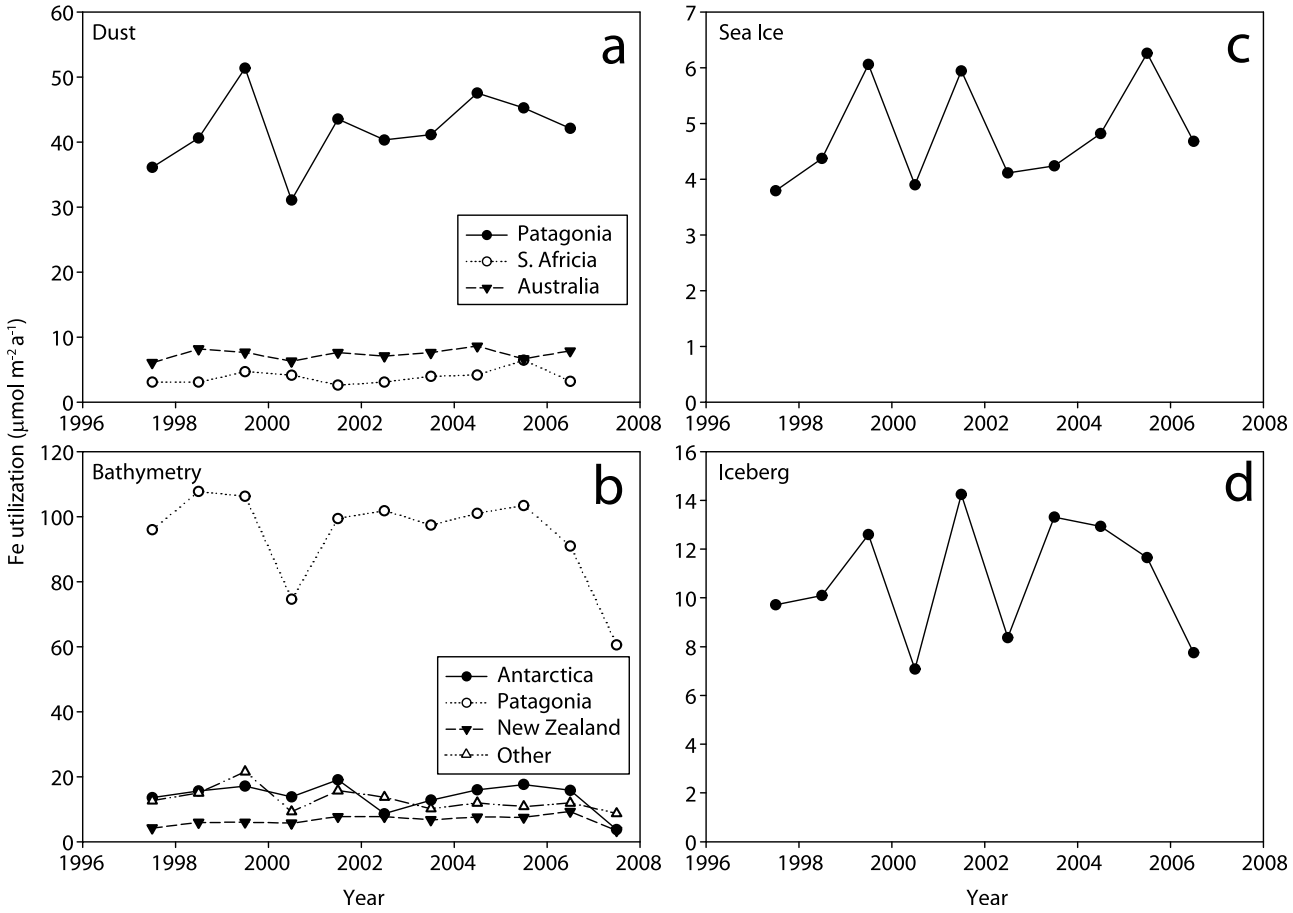

Figure 10. Fe utilization per unit area (μmol m^{-2} a^{-1}) for (a) dust maps; (b) bathymetry maps (sediment resuspension in waters <1000 m depth); (c) sea-ice retreat (MIZ); (d) ice-berg drift and melt.

than that reported by *Fung et al.* [2000] (12×10^9 mol Fe a^{-1}). However, a direct comparison is problematic as *Fung et al.* [2000] excluded the coastal ocean (i.e., <200 m depth and <800 km from shore, see Figure S4 in Text S2 of the auxiliary material) due to uncertainties at that time in Fe supply to these nearshore waters. We rescaled our estimate of Southern Ocean Fe demand (Figure 2) using the areal extent defined by *Fung et al.* [2000] (Figure S4 in Text S2 of the auxiliary material) and this resulted in a decreased estimate of $\sim 2.1 \times 10^8$ mol Fe a^{-1} (i.e., 60 fold less than *Fung et al.* [2000]) for that subset of Southern Ocean waters.

[34] Our estimate of a Southern Ocean phytoplankton Fe utilization is much less than that reported by *Fung et al.* [2000], which has implications for the biogeochemical modeling of this polar region. Our Fe utilization estimate is based on recently available Southern Ocean algal Fe:C ratios and a regionally validated NPP remote-sensing algorithm, whereas *Fung et al.* [2000] employed Fe:C ratios for temperate diatoms from *Sunda and Huntsman* [1995] (in conjunction with some rescaling using the Moss Landing Marine Lab data sets in *Johnson et al.* [1997]). *Fung et al.* [2000] also applied a global NPP algorithm [*Behrenfeld and Falkowski*, 1997] to estimate the phytoplankton Fe utilization. This global NPP algorithm when applied to Southern Ocean waters provides estimates of NPP that are 1.07 times higher (NB only cloud-free pixels were intercompared), and have a mean excess of 47 mg C m^{-2} d^{-1} relative to the *Arrigo et al.* [2008] NPP algorithm. Thus, the collective differences in the Fe:C ratios (i.e., temperate versus polar diatoms), and to a lesser extent in the NPP algorithms employed in our study, relative to those used by *Fung et al.* [2000], explain this considerably lower phytoplankton Fe utilization that we report for Southern Ocean waters.

4.2. Comparing Fe Utilization With Supply From Different Mechanisms

[35] The circumpolar estimates of phytoplankton Fe utilization that we produced cannot readily be compared with that for Fe supply, since the latter estimate will be much less spatially resolved (Figure 5). Furthermore, major uncertainties exist regarding the geographical realm of influence of each supply term and in some cases, little is known about putative mechanisms such as Southern Ocean eddies (Table 2). Nevertheless, our initial comparisons between the magnitude of Fe utilization and supply revealed that they are of the same order, and specifically that both regional match-ups and comparisons of maps of regionally distinct Fe utilization with the Fe supply revealed no major mismatches between the magnitude of utilization and supply.

[36] The application of Fe utilization maps does offer insights into the relative roles of different Fe supply

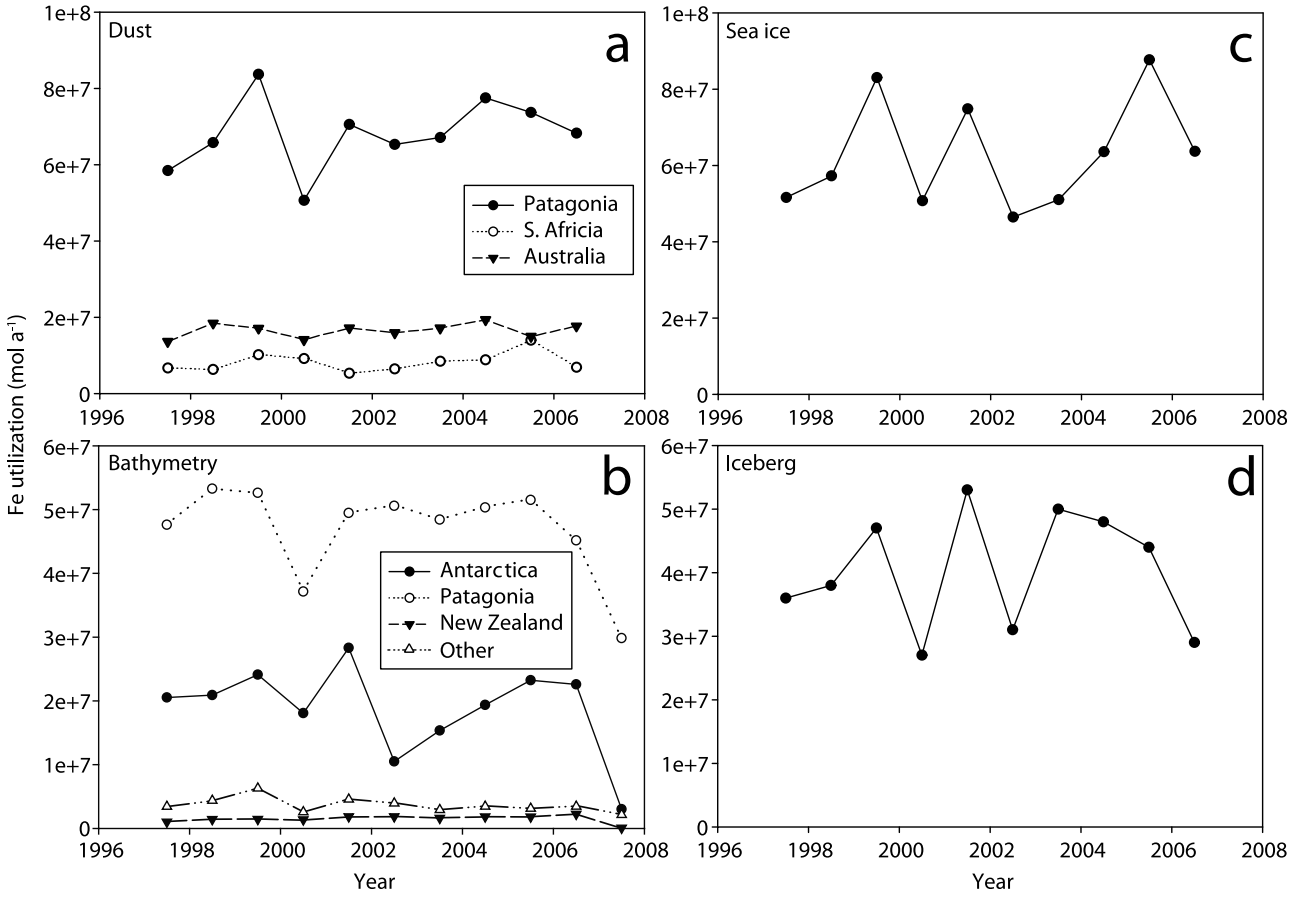

Figure 11. Fe utilization per unit area (mol a^{-1}) for (a) dust maps; (b) bathymetry maps (sediment resuspension in waters <1000 m depth); (c) sea-ice retreat; (d) ice-berg drift and melt.

mechanisms (Figures 10 and 11). There has been considerable debate about the importance of different mechanisms, with reports of a dominant mechanism, such as dust [*Cassar et al.*, 2007] or sedimentary Fe [*Tagliabue et al.*, 2009], or the role of multiple mechanisms [*Boyd and Mackie*, 2008]. This issue has yet to be resolved [*Cassar et al.*, 2008; *Moore and Braucher*, 2008; *Tagliabue et al.*, 2009]. Fe utilization maps may assist in teasing apart a range of issues that were identified by *Tagliabue et al.* [2009] and *Lancelot et al.* [2009], including the dispersion trajectory of Fe from point sources, regions that encounter Fe from multiple sources, and assessment of spatial heterogeneity of Fe supply between different regions of the Southern Ocean (for example those in which Fe is supplied by sea-ice melt and retreat).

[37] Our Fe utilization maps were subsampled and lateral changes in Fe utilization investigated to assess whether they follow generic rules for Fe dispersal, for example attenuation of Fe utilization downstream of a dust source where the 1/2 decrease distance concept of *Prospero et al.* [1989] should apply. We presented evidence that Fe utilization for aerosol Fe was consistent with a dust source and lateral attenuation signal in Australia and Southern Africa (Figure 6) whereas lateral trends east of Patagonia were consistent with multiple Fe supply mechanisms (overlap between masks was 6.1×10^5 km^2, Table S3 in Text S1 of the auxiliary material). The use of multiple maps, each corresponding to a different supply mechanism, enabled the calculation of the degree of spatial overlap between each map and hence address one of the concerns of *Tagliabue et al.* [2009].

[38] Little is known about the long distance dispersal patterns and supply of resuspended sedimentary Fe [*Charette et al.*, 2007; *Dulaiova et al.*, 2009]. 'Transects' through the Fe utilization maps (Figures 7–9) reveal that, unlike atmospheric dispersal and deposition [*Prospero et al.*, 1989], the offshore dispersal of resuspended Fe appears to be rapidly attenuated, probably due to both utilization and vertical settling of sedimentary Fe in the upper ocean over tens of kilometers. Similarly, by subsampling Fe utilization maps for the circumpolar sea-ice map, regions that support low, intermediate, and high phytoplankton Fe utilization [cf. *Lancelot et al.*, 2009] can be identified and the reasons for such patterns (e.g., differences in the localized Fe sources incorporated into the sea-ice based on mineralogy, solubility, and ocean versus glacial Fe inputs to the sea-ice) can be explored. By increasing our understanding of the geographical realm of influence and overlap of different supply terms, we will eventually be able to improve the accuracy of the simplistic circumpolar supply map presented in our study.

4.3. Why is Fe Utilization Relatively Constant Between Years?

[39] One of the most striking trends in the time series of both circumpolar and regional Fe utilization for Southern Ocean waters is that it changes little between years (Figure 2a

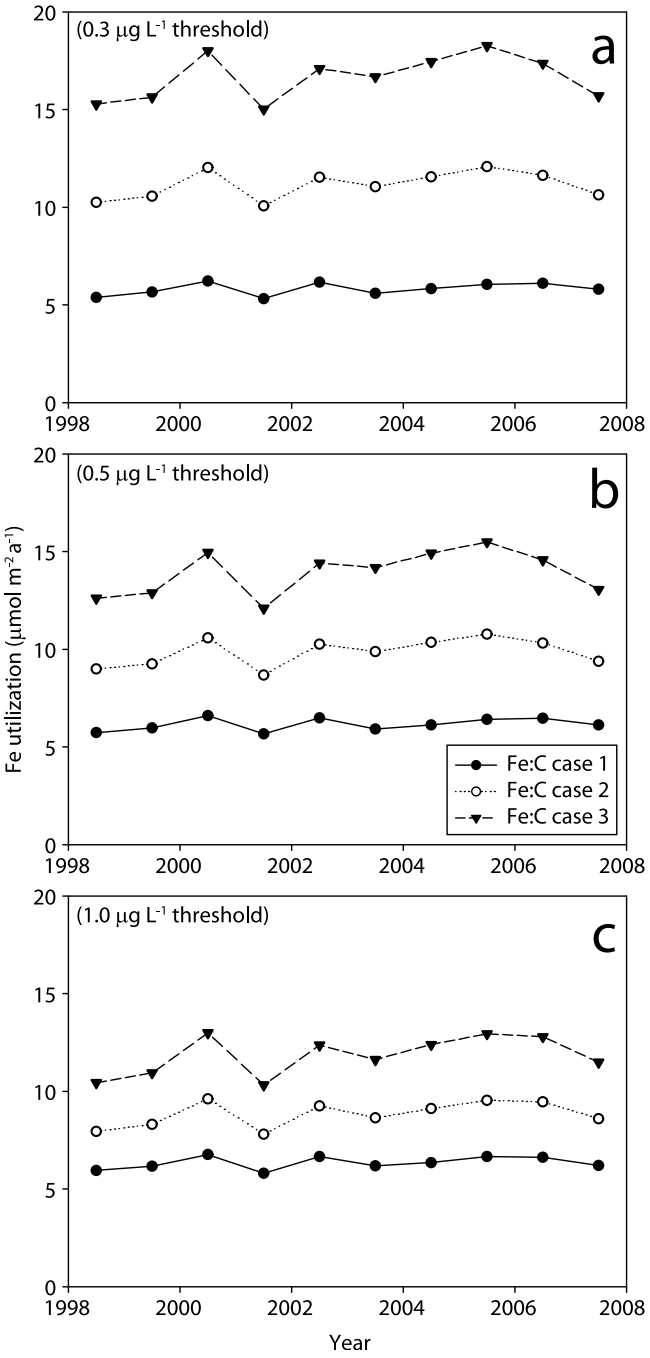

Figure 12. Sensitivity analysis on how annual Fe utilization is altered by employing different Fe:C ratios for phytoplankton and/or different low versus high thresholds for (a) 0.3 μg chl *a* L^{-1}; (b) 0.5 μg chl *a* L^{-1}; (c) 1.0 μg chl *a* L^{-1} for the three phytoplankton Fe:C scenarios given in Tables 1a and 1b.

and Figure S5 in Text S2 of the auxiliary material). This invariance over a decade in Fe utilization also characterizes subsets of the circumpolar data sets, such as the maps that relate to particular supply mechanisms like aerosol, sedimentary and sea-ice derived Fe. In contrast, the few comprehensive time series data that are available for the interannual variability in Fe supply from different mechanisms reveal large interannual variability for some mechanisms (such as aerosol Fe) but not for others (e.g., sea-ice melt and retreat) (Table 3). *Mackie et al.* [2008] report up to eightfold interannual variability in Australian dust activity (based on a proven proxy – the Dust Storm Index) over the period 1960 to 2010. In Patagonia, *Gaiero et al.* [2003] observed considerable seasonal (i.e., over the phytoplankton growth season from October to March) and inter-site variability in dust fluxes at three sites that supply Southern Ocean waters. However, despite this indirect evidence for interannual variability in aerosol Fe supplies, particularly in influential regions such as Patagonia, uncertainties exist as to how such variability will be altered by long-range dispersal and eventual deposition into the ocean. In contrast, *Stammerjohn et al.* [2008] saw little year-to-year changes in the areal extent of sea-ice extent (mean 1.38×10^7 km^2 (standard deviation = 8.4×10^5 km^2 (n-1 = 9)). However, the relationship between Fe supply and sea-ice areal extent may be complex given the observed heterogeneity in the Fe content of sea-ice between regions [*Lancelot et al.*, 2009] (Figure 8). Thus, based on the data assembled in Table 3, on the interannual variability in Fe supply, it is premature to make more than an initial comparison between year-to-year variability in Fe utilization versus Fe supply.

[40] The lack of evidence of interannual variability in Fe utilization may be due to the wide range of Fe supply mechanisms in the Southern Ocean, in particular if each mechanism has different environmental driver(s). The evidence we present of the geographical overlap in supply mechanisms (Table S3 in Text S1 of the auxiliary material), may result in a buffering effect. For example, if there is interannual variability in one mechanism that leads to decreased supply, it may be offset by concurrent increases in other supply mechanisms from the cryosphere, atmosphere, and/or hydrosphere.

[41] Such low interannual variability in Fe utilization may also be due to artifacts associated with the role of phytoplankton Fe physiology in setting chlorophyll concentration (i.e., a biomass proxy). The physiological alteration of chlorophyll concentration may offset changes in chlorophyll that are driven by modification of phytoplankton biomass [*Dierssen*, 2010]. This offsetting could account for reports of little change in phytoplankton stocks – based on remotely sensed chlorophyll – despite marked changes in seasonal mixed-layer depth in some Southern Ocean basins [*Sallée et al.*, 2010]. Moreover, *Arrigo et al.* [2008] report changes of ~15% in NPP in Southern Ocean waters over a decade. It is not possible to comment on whether the invariance in phytoplankton Fe utilization causes little change in NPP between years, as we used this NPP archive in conjunction with a range of Fe:C ratios for different algal groups. However, either the supply of Fe to Southern Ocean waters is not a key determinant of NPP or a series of artifacts (listed previously) may be masking or damping interannual variability in both Fe utilization and NPP and for Fe-replete and deplete waters.

4.4. Fe utilization and Supply in a Changing Southern Ocean

[42] The Southern Ocean is thought to be particularly sensitive to climate change [*Marinov et al.*, 2006] and is the only HNLC region where the cryosphere plays a role in Fe

supply. It is also a region where changes in Fe supply over millennia have played a disproportionate role in global climate [*Martinez-Garcia et al.*, 2011]. The present study, by jointly examining spatial and temporal trends in both Fe utilization and supply for as many supply mechanisms as possible, reveals some of the processes that may influence a changing Southern Ocean. For example, climate change mediated changes to the mixed layer depth and underwater light climate due to reduced sea-ice cover will increase Fe utilization in some regions in the future. There is also some indirect evidence that supply mechanisms that presently exhibit high interannual variability, such as Australian dust [*Mackie et al.*, 2008], presumably in response to climate variability, might also be expected to be altered more by a changing Southern Ocean than those that exhibit little interannual variability.

[43] There are also modeling projections, such as the enhancement of eddy-induced transport around the ACC in the coming decades [*Wang et al.*, 2011], but to date, there are no comprehensive data on how eddies influence Fe supply in the Southern Ocean, although studies from other regions suggest that this may well be the case [*Xiu et al.*, 2011]. The value of the Fe utilization map approach can be further exploited to reduce uncertainties in how Fe supply and utilization will be altered in a changing Southern Ocean. In particular, these utilization maps provide important spatial resolution to assess patterns in Fe utilization that will assist us in better understanding how a spatial and temporal changes in a wide range of distinct supply mechanisms might manifest themselves as a biological imprint in the waters, regions, and sub-regions of the Southern Ocean.

[44] **Acknowledgments.** We thank the Ministry of Science and Innovation New Zealand and Royal Society Marsden Fund for support of P.B. and R.S., respectively. We are grateful to Alessandro Tagliabue (University of Capetown) for providing estimates of the flux of hydrothermal Fe into the surface ocean based on the model used in the *Tagliabue et al.* [2010] study. Lisa Bucke (University of Otago) kindly provided the Fe supply map in Figure 5b. The constructive comments of two anonymous reviewers and from Mak Saito also helped to improve this manuscript.

References

Adams, D. K., D. J. McGillicuddy Jr., L. Zamudio, A. M. Thurnherr, X. Lang, O. Rouxel, C. R. German, and L. S. Mullineaux (2011), Surface-generated mesoscale eddies transport deep-sea products from hydrothermal vents, *Science*, *332*, 580–583, doi:10.1126/science.1201066.

Ardelan, M. V., O. Holm-Hansen, C. D. Hewes, C. S. Reiss, N. S. Silva, H. Dulaiova, E. Steinnes, and E. Sakshaug (2010), Natural iron enrichment around the Antarctic Peninsula in the Southern Ocean, *Biogeosciences*, *7*, 11–25, doi:10.5194/bg-7-11-2010.

Arrigo, K. R., G. R. DiTullio, R. B. Dunbar, M. P. Lizotte, D. H. Robinson, M. VanWoert, and D. L. Worthen (2000), Phytoplankton taxonomic variability and nutrient utilization and primary production in the Ross Sea, *J. Geophys. Res.*, *105*, 8827–8846, doi:10.1029/1998JC000289.

Arrigo, K. R., G. L. van Dijken, and S. Bushinsky (2008), Primary production in the Southern Ocean, 1997–2006, *J. Geophys. Res.*, *113*, C08004, doi:10.1029/2007JC004551.

Baker, A. R., and P. L. Croot (2010), Atmospheric and marine controls on aerosol iron solubility in seawater, *Mar. Chem.*, *120*, 4–13, doi:10.1016/j.marchem.2008.09.003.

Behrenfeld, M. J., and P. G. Falkowski (1997), Photosynthetic rates derived from satellite-based chlorophyll concentration, *Limnol. Oceanogr.*, *42*(1), 1–20, doi:10.4319/lo.1997.42.1.0001.

Blain, S., et al. (2007), Effect of natural iron fertilization on carbon sequestration in the Southern Ocean, *Nature*, *446*, 1070–1074.

Bowie, A. R., D. Lannuzel, T. A. Remenyi, T. Wagener, P. J. Lam, P. W. Boyd, C. Guieu, A. T. Townsend, and T. W. Trull (2009), Biogeochemical iron budgets of the Southern Ocean south of Australia: Decoupling of iron and nutrient cycles in the subantarctic zone by the summertime supply, *Global Biogeochem. Cycles*, *23*, GB4034, doi:10.1029/2009GB003500.

Boyd, P. W., and M. J. Ellwood (2010), The biogeochemical cycle of iron in the ocean, *Nat. Geosci.*, *3*, 675–682, doi:10.1038/ngeo964.

Boyd, P. W., and D. Mackie (2008), Comment on the Southern Ocean biological response to aeolian iron deposition, *Science*, *319*, 159, doi:10.1126/science.1149884.

Boyd, P. W., et al. (1999), Role of iron, light, and silicate in controlling algal biomass in subantarctic waters SE of New Zealand, *J. Geophys. Res.*, *104*, 13,395–13,408, doi:10.1029/1999JC900009.

Boyd, P. W., et al. (2005), FeCycle: Attempting an iron biogeochemical budget from a mesoscale SF_6 tracer experiment in unperturbed low iron waters, *Global Biogeochem. Cycles*, *19*, GB4S20, doi:10.1029/2005GB002494.

Boyd, P. W., et al. (2007), Mesoscale iron enrichment experiments 1993–2005: Synthesis and future directions, *Science*, *315*, 612–617, doi:10.1126/science.1131669.

Boyd, P. W., D. S. Mackie, and K. A. Hunter (2010), Aerosol iron deposition to the surface ocean—Modes of iron supply and biological responses, *Mar. Chem.*, *120*, 128–143, doi:10.1016/j.marchem.2009.01.008.

Cassar, N., M. L. Bender, B. A. Barnett, S. Fan, W. J. Moxim, H. Levy, and B. Tilbrook (2007), The Southern Ocean biological response to aeolian iron deposition, *Science*, *317*, 1067–1070, doi:10.1126/science.1144602.

Cassar, N., M. L. Bender, B. A. Barnett, S. Fan, W. J. Moxim, H. Levy, and B. Tilbrook (2008), Response to comment on the Southern Ocean biological response to aeolian iron deposition, *Science*, *319*, 159, doi:10.1126/science.1150011.

Charette, M. A., M. E. Gonneea, P. Morris, P. Statham, G. Fones, H. Planquette, I. Salter, and A. N. Garabato (2007), Radium isotopes as tracers of iron sources fueling a Southern Ocean phytoplankton bloom, *Deep Sea Res., Part II*, *54*, 1989–1998, doi:10.1016/j.dsr2.2007.06.003.

Chavez, F. P., P. G. Strutton, C. E. Friederich, R. A. Feely, G. C. Feldman, D. C. Foley, and M. J. McPhaden (1999), Biological and chemical response of the equatorial Pacific Ocean to the 1997–98 El Niño, *Science*, *286*, 2126–2131, doi:10.1126/science.286.5447.2126.

Daly, K., W. Smith Jr., G. Johnson, G. DiTullio, D. Jones, C. Mordy, R. Feely, D. Hansell, and J. Z. Zhang (2001), Hydrography, nutrients, and carbon pools in the Pacific sector of the Southern Ocean: Implications for carbon flux, *J. Geophys. Res.*, *106*(C4), 7107–7124, doi:10.1029/1999JC000090.

de Baar, H. J. W., et al. (1995), Importance of iron for plankton blooms and carbon-dioxide drawdown in the Southern Ocean, *Nature*, *373*, 412–415, doi:10.1038/37341.

Dierssen, H. M. (2010), Perspectives on empirical approaches for ocean color remote sensing of chlorophyll in a changing climate, *Proc. Natl. Acad. Sci. U. S. A.*, *107*, 17,073-17,078, doi:10.1073/pnas.0913800107.

Dulaiova, H., M. V. Ardelan, P. B. Henderson, and M. A. Charette (2009), Shelf-derived iron inputs drive biological productivity in the southern Drake Passage, *Global Biogeochem. Cycles*, *23*, GB4014, doi:10.1029/2008GB003406.

Fung, I. Y., S. K. Meyn, I. Tegen, S. C. Doney, J. G. John, and J. K. B. Bishop (2000), Iron supply and utilization in the upper ocean, *Global Biogeochem. Cycles*, *14*(1), 281–295, doi:10.1029/1999GB900059.

Gaiero, D. M., J.-L. Probst, P. J. Depetris, S. M. Bidart, and L. Leleyter (2003), Iron and other transition metals in Patagonian riverborne and windborne materials: Geochemical control and transport to the southern South Atlantic Ocean, *Geochim. Cosmochim. Acta*, *67*(19), 3603–3623, doi:10.1016/S0016-7037(03)00211-4.

Hamme, R. C., et al. (2010), Volcanic ash fuels anomalous plankton bloom in subarctic northeast Pacific, *Geophys. Res. Lett.*, *37*, L19604, doi:10.1029/2010GL044629.

Jickells, T. D., et al. (2005), Global iron connections between desert dust, ocean biogeochemistry, and climate, *Science*, *308*(5718), 67–71, doi:10.1126/science.1105959.

Johnson, K. S., R. M. Gordon, and K. H. Coale (1997), What controls dissolved iron concentrations in the world ocean?, *Mar. Chem.*, *57*, 137–161, doi:10.1016/S0304-4203(97)00043-1.

Lancelot, C., A. de Montety, H. Goosse, S. Becquevort, V. Schoemann, B. Pasquer, and M. Vancoppenolle (2009), Spatial distribution of the iron supply to phytoplankton in the Southern Ocean: A model study, *Biogeosciences*, *6*, 2861–2878, doi:10.5194/bg-6-2861-2009.

Lannuzel, D., V. Schoemann, J. de Jong, J. L. Tison, and L. Chou (2007), Distribution and biogeochemical behaviour of iron in the East Antarctic sea ice, *Mar. Chem.*, *106*, 18–32, doi:10.1016/j.marchem.2006.06.010.

Mackie, D. S., P. W. Boyd, G. H. McTainsh, N. W. Tindale, T. K. Westberry, and K. A. Hunter (2008), Biogeochemistry of iron in Australian dust: From eolian uplift to marine uptake, *Geochem. Geophys. Geosyst.*, *9*, Q03Q08, doi:10.1029/2007GC001813.

Mahowald, N. M., et al. (2005), Atmospheric global dust cycle and iron inputs to the ocean, *Global Biogeochem. Cycles*, *19*, GB4025, doi:10.1029/2004GB002402.

Marinov, I., A. Gnanadesikan, J. R. Toggweiler, and J. L. Sarmiento (2006), The Southern Ocean biogeochemical divide, *Nature*, *441*, 964–967, doi:10.1038/nature04883.

Martin, J. H., R. M. Gordon, S. Fitzwater, and W. W. Broenkow (1989), VERTEX: Phytoplankton/iron studies in the Gulf of Alaska, *Deep Sea Res., Part A*, *36*, 649–680, doi:10.1016/0198-0149(89)90144-1.

Martinez-Garcia, A., A. Rosell-Mele, S. L. Jaccard, W. Geibert, D. M. Sigman, and G. H. Haug (2011), Southern Ocean dust–climate coupling over the past four million years, *Nature*, *476*, 312–315, doi:10.1038/nature10310.

McKay, R. M. L., S. W. Wilhelm, J. Hall, D. A. Hutchins, M. M. D. Al-Rshaidat, C. E. Mioni, S. Pickmere, D. Porta, and P. W. Boyd (2005), Impact of phytoplankton on the biogeochemical cycling of iron in subantarctic waters southeast of New Zealand during FeCycle, *Global Biogeochem. Cycles*, *19*, GB4S24, doi:10.1029/2005GB002482.

Measures, C. I., and S. Vink (2001), Dissolved Fe in the upper waters of the Southern Ocean during the 1997/98 US-JGOFS cruises, *Deep Sea Res., Part II*, *48*, 2787–2809.

Moore, J. K., and M. R. Abbott (2000), Phytoplankton chlorophyll distributions and primary production in the Southern Ocean, *J. Geophys. Res.*, *105*, 28,709–28,722, doi:10.1029/1999JC000043.

Moore, J. K., and O. Braucher (2008), Sedimentary and mineral dust sources of dissolved iron to the world ocean, *Biogeosciences*, *5*, 631–656, doi:10.5194/bg-5-631-2008.

Moore, J. K., S. C. Doney, and K. Lindsay (2004), Upper ocean ecosystem dynamics and iron cycling in a global three-dimensional model, *Global Biogeochem. Cycles*, *18*, GB4028, doi:10.1029/2004GB002220.

Pabi, S., G. L. van Dijken, and K. R. Arrigo (2008), Primary production in the Arctic Ocean, 1998–2006, *J. Geophys. Res.*, *113*, C08005, doi:10.1029/2007JC004578.

Pollard, R. T., et al. (2009), Southern Ocean deep-water carbon export enhanced by natural iron fertilization, *Nature*, *457*, 577–580, doi:10.1038/nature07716.

Prospero, J., M. Uematsu, and D. Savoie (1989), Mineral aerosol transport to the Pacific Ocean, in *Chemical Oceanography*, vol. 10, edited by J. P. Riley and R. Chester, pp. 188–216, Elsevier, New York.

Raiswell, R., L. G. Benning, M. Tranter, and S. Tulaczyk (2008), Bioavailable iron in the Southern Ocean: The significance of the iceberg conveyor belt, *Geochem. Trans.*, *9*, 7, doi:10.1186/1467-4866-9-7.

Sallée, J. B., K. G. Speer, and S. R. Rintoul (2010), Zonally asymmetric response of the Southern Ocean mixed-layer depth to the Southern Annular Mode, *Nat. Geosci.*, *3*, 273–279, doi:10.1038/ngeo812.

Sarthou, G., K. R. Timmermans, S. Blain, and P. Tréguer (2005), Growth physiology and fate of diatoms in the ocean: A review, *J. Sea Res.*, *53*, 25–42, doi:10.1016/j.seares.2004.01.007.

Sarthou, G., et al. (2008), The fate of biogenic iron during a phytoplankton bloom induced by natural fertilisation: Impact of copepod grazing, *Deep Sea Res., Part II*, *55*, 734–751, doi:10.1016/j.dsr2.2007.12.033.

Schodlok, M. P., H. H. Hellmer, G. Rohardt, and E. Fahrbach (2006), Weddell Sea iceberg drift: Five years of observations, *J. Geophys. Res.*, *111*, C06018, doi:10.1029/2004JC002661.

Sedwick, P. N., et al. (2011), Early season depletion of dissolved iron in the Ross Sea polynya: Implications for iron dynamics on the Antarctic continental shelf, *J. Geophys. Res.*, *116*, C12019, doi:10.1029/2010JC006553.

Shaw, T. J., R. Raiswell, C. R. Hexel, H. P. Vu, W. S. Moore, R. Dudgeon, and K. L. Smith (2011), Input, composition and potential impact of terrigenous material from free-drifting icebergs in the Weddell Sea, *Deep Sea Res., Part II*, *58*(11–12), 1376–1383, doi:10.1016/j.dsr2.2010.11.012.

Smith, K. L., Jr. (2011), Free-drifting icebergs in the Southern Ocean: An overview, *Deep Sea Res., Part II*, *58*, 1277–1284, doi:10.1016/j.dsr2.2010.11.003.

Smith, W. O., Jr., J. Marra, M. R. Hiscock, and R. T. Barber (2000), The seasonal cycle of phytoplankton biomass and primary productivity in the Ross Sea, Antarctica, *Deep Sea Res., Part II*, *47*, 3119–3140, doi:10.1016/S0967-0645(00)00061-8.

Sokolov, S., and S. R. Rintoul (2007), On the relationship between fronts of the Antarctic Circumpolar Current and surface chlorophyll concentrations in the Southern Ocean, *J. Geophys. Res.*, *112*, C07030, doi:10.1029/2006JC004072.

Stammerjohn, S. E., D. G. Martinson, R. C. Smith, X. Yuan, and D. Rind (2008), Trends in Antarctic annual sea ice retreat and advance and their relation to El Niño–Southern Oscillation and Southern Annular Mode variability, *J. Geophys. Res.*, *113*, C03S90, doi:10.1029/2007JC004269.

Strzepek, R. F., M. T. Maldonado, K. A. Hunter, R. D. Frew, and P. W. Boyd (2011), Adaptive strategies by Southern Ocean phytoplankton to lessen iron limitation: Uptake of organically complexed iron and reduced cellular iron requirements, *Limnol. Oceanogr.*, *56*, 1983–2002, doi:10.4319/lo.2011.56.6.1983.

Stuart, K. M., and D. G. Long (2011), Tracking large tabular icebergs using the Sea Winds Ku-band microwave scatterometer, *Deep Sea Res., Part II*, *58*(11–12), 1285–1300, doi:10.1016/j.dsr2.2010.11.004.

Sullivan, C. W., K. R. Arrigo, C. R. McClain, J. C. Comiso, and J. Firestone (1993), Distributions of phytoplankton blooms in the Southern Ocean, *Science*, *262*, 1832–1837, doi:10.1126/science.262.5141.1832.

Sunda, W. G., and S. A. Huntsman (1995), Iron uptake and growth limitation in oceanic and coastal phytoplankton, *Mar. Chem.*, *50*, 189–206, doi:10.1016/0304-4203(95)00035-P.

Tagliabue, A., L. Bopp, and O. Aumont (2009), Evaluating the importance of atmospheric and sedimentary iron sources to Southern Ocean biogeochemistry, *Geophys. Res. Lett.*, *36*, L13601, doi:10.1029/2009GL038914.

Tagliabue, A., L. Bopp, J.-C. Dutay, A. R. Bowie, F. Chever, P. Jean-Baptiste, E. Bucciarelli, D. Lannuzel, T. Remenyi, and G. Sarthou (2010), Hydrothermal contribution to the oceanic dissolved iron inventory, *Nat. Geosci.*, *3*(4), 252–256, doi:10.1038/ngeo818.

Tréguer, P., and G. Jacques (1992), Dynamics of nutrients and phytoplankton, and fluxes of carbon, nitrogen, and silicon in the Antarctic Ocean, *Polar Biol.*, *12*, 149–162, doi:10.1007/BF00238255.

Twining, B. S., S. B. Baines, N. S. Fisher, and M. R. Landry (2004), Cellular iron contents of plankton during the Southern Ocean Iron Experiment (SOFeX), *Deep Sea Res., Part I*, *51*, 1827–1850, doi:10.1016/j.dsr.2004.08.007.

Wagener, T., C. Guieu, R. Losno, S. Bonnet, and N. Mahowald (2008), Revisiting atmospheric dust export to the Southern Hemisphere ocean: Biogeochemical implications, *Global Biogeochem. Cycles*, *22*, GB2006, doi:10.1029/2007GB002984.

Wang, Z., T. Kuhlbrodt, and M. P. Meredith (2011), On the response of the Antarctic Circumpolar Current transport to climate change in coupled climate models, *J. Geophys. Res.*, *116*, C08011, doi:10.1029/2010JC006757.

Xiu, P., A. P. Palacz, F. Chai, E. G. Roy, and M. L. Wells (2011), Iron flux induced by Haida eddies in the Gulf of Alaska, *Geophys. Res. Lett.*, *38*, L13607, doi:10.1029/2011GL047946.